Heliyon 9 (2023) e17718

Contents lists available at ScienceDirect

Heliyon

journal homepage: www.cell.com/heliyon

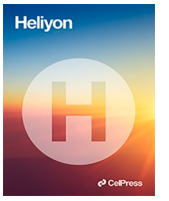

Review article

An overview of 3D printed metal implants in orthopedic applications: Present and future perspectives

Yuanhao Wu [a], Jieying Liu [a], Lin Kang [a], Jingjing Tian [a], Xueyi Zhang [a], Jin Hu [a], Yue Huang [b], Fuze Liu [b], Hai Wang [b,*], Zhihong Wu [a,c,**]

[a] *Medical Research Center, State Key Laboratory of Complex Severe and Rare Diseases, Peking Union Medical College Hospital, Peking Union Medical College and Chinese Academy of Medical Sciences, Beijing, 100730, China*
[b] *Department of Orthopedic Surgery, Peking Union Medical College Hospital, Peking Union Medical College and Chinese Academy of Medical Sciences, Beijing, 100730, China*
[c] *Beijing Key Laboratory for Genetic Research of Bone and Joint Disease, Beijing, China*

ARTICLE INFO

Keywords:
3D printing
Implants
Orthopedic application
Clinic trials
Regulation

ABSTRACT

With the ability to produce components with complex and precise structures, additive manufacturing or 3D printing techniques are now widely applied in both industry and consumer markets. The emergence of tissue engineering has facilitated the application of 3D printing in the field of biomedical implants. 3D printed implants with proper structural design can not only eliminate the stress shielding effect but also improve in vivo biocompatibility and functionality. By combining medical images derived from technologies such as X-ray scanning, CT, MRI, or ultrasonic scanning, 3D printing can be used to create patient-specific implants with almost the same anatomical structures as the injured tissues. Numerous clinical trials have already been conducted with customized implants. However, the limited availability of raw materials for printing and a lack of guidance from related regulations or laws may impede the development of 3D printing in medical implants. This review provides information on the current state of 3D printing techniques in orthopedic implant applications. The current challenges and future perspectives are also included.

1. Introduction

Additive manufacturing (AM), also known as rapid prototyping (RP) or Three-Dimensional printing (3D Printing), was invented in the 1980s, with Charles Hull developing the world's first commercial 3D printer in 1986. In 2009, 3D printing was defined by the ASTM International Committee as the "process of joining materials to make objects from 3-dimensional (3D) model data, usually layer by layer, as opposed to subtractive manufacturing methodologies" [1,2].

It is an advanced manufacturing process that is distinct from conventional manufacturing techniques like casting, forging, and machining. For 3D printing, the original data required can be gathered from Computed Tomography (CT) scanning or Magnetic

* Corresponding author. Department of Orthopedic Surgery, Peking Union Medical College Hospital, Peking Union Medical College and Chinese Academy of Medical Sciences, Beijing, 100730, China.
** Corresponding author. Medical Research Center, State Key Laboratory of Complex Severe and Rare Diseases, Peking Union Medical College Hospital, Peking Union Medical College and Chinese Academy of Medical Sciences, Beijing, 100730, China.
E-mail addresses: wanghai907@hotmail.com (H. Wang), 13911071856@126.com (Z. Wu).

https://doi.org/10.1016/j.heliyon.2023.e17718
Received 22 December 2022; Received in revised form 12 June 2023; Accepted 26 June 2023
Available online 29 June 2023

Resonance Imaging (MRI), and 3D modeling design can be achieved with the aid of 3D Computer-Aided Design (CAD) software. Once the preparation procedures are completed, the printing process can be done bottom-up in one step. Unlike conventional manufacturing, 3D printing is a material-specific and design-specific system, thus making it possible to fabricate components with complex geometric shapes without requiring tooling or molds when printing. Other advantages like cost-effectiveness, freedom of design, and controllable precision have attracted considerable attention in both industry and consumer markets [3,4]. In the past few decades, 3D printing has reached significant advances in printing methods as an emerging fabrication technique [5–7]. The cost of 3D printing has decreased with technological developments over time. It provides manufacturers with great design freedom for printed products while lowering customization costs compared to conventional manufacturing methods. In the 1990s, the advent of tissue engineering led to the application of biomedical scaffold implants with appropriate structural design for repairing or replacing injured or diseased tissues [8]. However, manufacturing scaffolds with complex geometric structures for individual patients using traditional machining methods was challenging. The possibility of using medical images to create customized implants with controlled gradient structure, porosity, and pore size demonstrated the potential of 3D printing technology in biomedical applications, especially in orthopedic surgery. Today, many clinical trials have been conducted with 3D printed implants in orthopedic applications. Surgeons and engineers are attracted to this technology and have made considerable efforts to improve clinical outcomes.

In this present review, our primary goal is to summarize clinical examples of 3D printing applications in orthopedic implants. Additionally, we provide a brief overview of the data acquisition or implant design processes. We also discuss the current challenges and future prospects in this field. Our intention is to inform both surgeons and engineers and inspire them to further promote the use of 3D printing techniques in clinical applications.

2. Fabrication procedure of 3D printed orthopedic implants

The use of 3D printing for orthopedic implant applications typically involves four basic procedures: acquiring raw medical data, preprocessing, printing the components, and post-processing. Once the finished components have been properly sterilized, they can be applied in the desired clinical applications. Fig. 1 provides a brief illustration of the typical process for biomedical applications.

2.1. Data acquisition and processing

Before printing orthopedic implants, the first step is to create printing models using clinical images. These images, derived from X-ray imaging, CT, MRI, and ultrasound (Fig. 2a), should have appropriate resolution for generating 3D printing models. Images with low resolution may produce inaccurate geometry parameters in the resulting models. Nowadays, images with ultra-high spatial resolution of 400–600 μm can be achieved for clinical use [9].

After obtaining the initial radiological scan images in raw digital imaging and communications in medicine (DICOM) format, they are converted into a CAD file using various 3D software programs such as Osirix, MeshLab, and 3D Slicer. These programs support 3D reconstruction of the images. Additionally, advanced post-data processing algorithms are developed to improve reconstruction results for low-resolution or non-enhanced images [10].

The converted image files undergo segmentation and surface preparation processes to select or isolate the region of interest (ROI) (Fig. 2b) and generate the surface mesh (Fig. 2c), respectively. Once the segmentation and mesh generation processes are complete, these data are usually saved in standard tessellation language (STL) file format (Fig. 2d) in order to be used by 3D printers. Different printing techniques and 3D print machines can then be used to print the desired components. In situations where 3D reconstruction of raw images for implantation sites is unavailable, the unaffected contralateral side can be mirrored to generate the STL files [11,12]. Additionally, in some cases, raw images are not necessary, and the intended implant models can be directly created from CAD software [13–15].

The conventional CAD-to-STL based pipeline is suitable for fulfilling the demand for 3D printed implants with simple geometries where the number of mesh triangles is below 1 million. However, for implants with highly complex structures and intricate details, the number of triangles can become tremendously large, resulting in significant time and computer memory consumption for processing and printing. To address this issue, Ding et al. proposed a STL-free method which integrated implicit solid remodeling for design and direct slicing for printing without any STL-related representation or intermediate steps related to STL meshes. This approach reduces

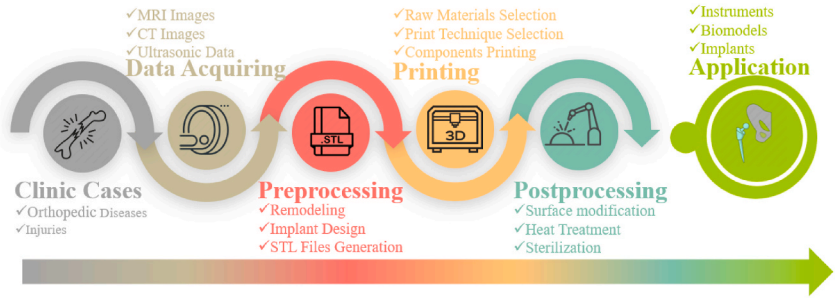

Fig. 1. Typical process for the design and application of 3D print implants in biomedical application.

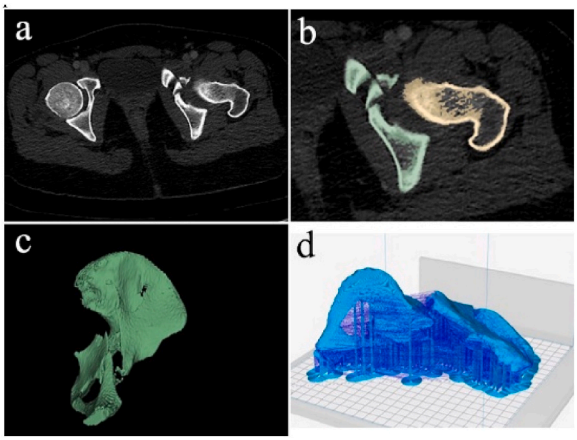

Fig. 2. Medical images acquiring and 3D model regeneration. a) DICOM images from CT scanning, b) segmentation of the RIO, c) 3D meshes of the ROI, d) slicing for printing [22], reprinted with permission.

both the memory usage and processing time. The new digital pipeline provides a novel way to design and print 3D printed implants [16].

As mentioned above, there are still multiple procedures that need to be completed before the implants can be printed. These processes, including printing hardware quality, reconstruction, segmentation, and surface extraction algorithms, can eventually influence the geometric accuracy of the final printed implants. Inaccuracies in different procedures can accumulate. A maximum length error of 2.3 mm (4.1%) was found in medical imaging acquisition and the end-use implant [17]. Liu et al. conducted a preliminary investigation on the geometric accuracy of 3D printed dental implants [18]. According to their results, the accuracy for the printed versus actual tooth, segmented versus actual tooth, and segmented versus printed tooth groups were 68.70 ± 5.63, 66.91 ± 10.51, and 90.59 ± 4.75, respectively. Thus, quality control during the entire procedure is important. Kopsacheilis et al. developed a simple, in-situ, automatic, vision-based, real-time monitoring system to detect errors during the 3D print process using a low-cost RGB-Depth camera and accelerometer [19].Improved segmentation and refinement algorithms can also be applied to balance accuracy and model complexity to improve model quality [20]. When compared to CT scan and computer numerical control (CNC) milling, cone beam computerized tomography (CBCT) segmentation showed the least distortion for printing the root analog implant [21].

2.2. Implants design

Bone is a natural reinforced concrete-like composite material with complex hierarchical porous structure, and act as load bearing tissue in human body. It consists of two main components: organic compounds such as collagen and fibrillin and inorganic minerals, predominantly hydroxyapatite (HA) [23]. Bone can be further categorized as cortical or cancellous bone. The cortical bone exhibits compact or solid state with a porosity of 3–5%, and the cancellous bone exhibits a porous network with a porosity ranging from 50 to 90% [24]. In the case of 3D printed bone implants, they should not only provide basic mechanical support but also promote regeneration of the injured bones. The design of architecture plays a crucial role in in vivo behavior. Successful 3D printed implants must meet several requirements, including biocompatibility, an optimal surface for cell attachment, a connected porous structure for cell ingrowth, and comparable mechanical properties to natural bone to minimize the stress shielding effect [25–27].

2.2.1. Pore size, porosity and interconnectivity

Bone exhibits a complex and heterogeneous porous anatomy structure with pore sizes ranging from macro to nano scale. Therefore, 3D printed implants should have similar porous structures in order to better mimic natural bones. When compared to traditional solid implants made from materials such as Ti, stainless steel, or Co–Cr, the macro or micro pore in 3D printed implants provide the space where cells, tissues, blood vessels and nerves can grow in. The interconnected pore network also facilitates sufficient permeability for the exchange of nutrients and metabolic waste between cells and the extracellular matrix (ECM), which favors the process of osteogenesis, including cell colonization, proliferation, differentiation, and ECM deposition [28,29]. It is widely recognized that pore size and porosity significantly affect the progression of osteogenesis [29,30]. Therefore, the pore size and porosity of 3D printed implants should be carefully designed to achieve optimal in vivo biological responses.

The optimal pore size for orthopedic implants is still a matter of controversy. It had been reported that the optimal pore size for mineralized bone ingrowth for porous scaffolds was 100–400 μm. However, Itala er al [31] found that there was no threshold value for new bone ingrowth for pore sizes ranging from 50 to 125 μm, as observed in non-loading conditions in rabbit bone regeneration models. According to Kuboki et al. [32], the optimal pore size for bone-forming efficacy in HA porous blocks is 300–400 μm and different pore sizes exhibit different functions. Smaller pores with a diameter of 90–120 μm tend to induce cartilage formation followed by new bone formation, while larger diameter (350 μm) induce direct bone formation. Taking the cell size into consideration, Karageorgiou et al. [24] suggested that the minimum requirement for pore sizes should be ~100 μm, and larger pore size like >300 μm

were recommended in order to improve new bone formation as well as the formation of capillaries. Taniguchi et al. [33] fabricated porous Ti scaffolds with pore size of 300, 600, 900 μm and porosity of 65%. After 2 weeks of implantation, scaffolds with a 600 μm pore diameter demonstrated a significantly higher fixation ability. After 4 weeks of implantation, bone growth in scaffolds with a 300 μm diameter was lower than that in the other implants. They concluded that scaffolds with 600 μm pore diameters were suitable for orthopedic implants. Similar results had also been reported in Ref. [34].

Ti6Al4V scaffolds printed via SLM (Selective Laser Melting) technique with proper mechanical property comparable to natural bones can be achieved (Fig. 3a and b). Although, small pore size (401 ± 26 μm) can facilitate cell seeding efficiency, it was observed that cell differentiation was not significantly affected by pore size (Fig. 3(b5-d5)). In order to improve bone ingrowth and bone-implant fixation stability, implants with an actual pore size of 607 ± 24 μm were found to be optimal based on in vivo studies (Fig. 3(b1-e1,b2-e2,b3-d3,b4-d4,b6-d6)) as illustrated in Fig. 3. Biodegradable scaffolds, on the other hand, researches suggested that smaller pore size can also suitable for bone ingrowth [35–37].

Bone regeneration in porous scaffolds relies on the recruitment and infiltration of cells from surrounding bone tissues and ECM. The porosity of the scaffolds determines the available space for cells and tissues to grow in [38]. Higher porosity generally facilitates the recruitment of cells, promotes the bone ingrowth and implant fixation with surrounding tissues [29,39,40]. Porosity can also affect the cellular response and tissue integration by changing the absorption of proteins and fluid shear forces [41,42]. However, a higher porosity does not guarantee more bone formation or vascularization because if the pores of the scaffold have limited interconnectivity, cellular migration and vascularization may be hindered [24]. In general, porosity of scaffolds should be more than 40% in order to ensure good biocompatibility [43]. Pore interconnectivity, also known as permeability, is another critical parameter for 3D printed scaffolds. Interconnected pores facilitate the transport of cells, nutrients, growth factors and flow of blood within the scaffolds. Permeability had also been reported to influence both in vitro and in vivo osteogenesis [44]. Kemppainen et al. [45] found that scaffold permeability affects the chondrogenic performance of chondrocytes and bone marrow stromal cells (BMSC) in opposite ways: the cartilaginous matrix production increased with the decrement of scaffold permeability, while the differentiation of BMSCs increased with an increment of permeability. Mitsak et al. [46] reported similar results. They observed that the poly-ϵ-caprolactone scaffolds with higher permeability showed enhanced bone penetration with blood vessel infiltration in immune-compromised mice four weeks after implantation.

It is important to note that there may be deviations between the designed nominal implants and the printed real implants. During

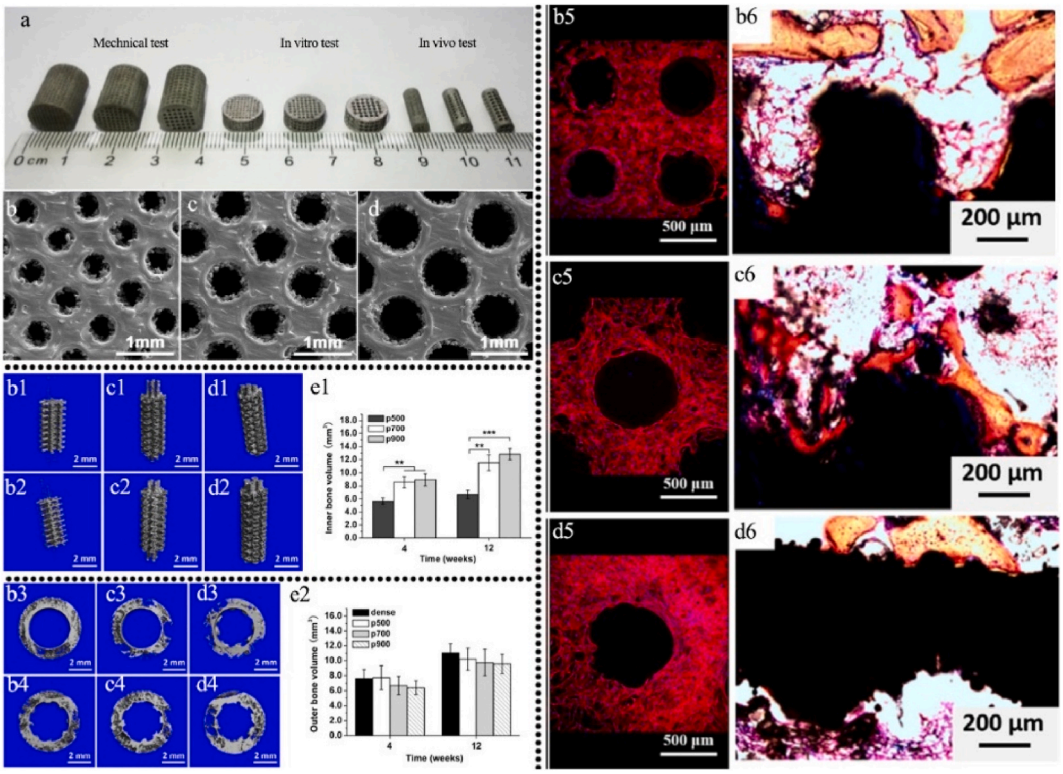

Fig. 3. Effect of pore size on in vivo osteogenesis of 3D printed scaffolds with different pore size [34]: a: 3D printed scaffolds for different tests, b: pore size 401 ± 26 μm, c: pore size 607 ± 24 μm, d: pore size 801 ± 33 μm; μ-CT analysis of inner bone formation after implantation for 4 (b1-d1) and 12 weeks (b2-d2), e1: quantitative analysis of inner new bone volume and outer bone formation after implantation for 4 (b3-d3) and 12 weeks (b4-d4), e2: Quantitative analysis of outer new bone volume; osteoblast adherence on the scaffolds on day 14 (b5-d5); Von-Gieson staining of osseointegration after implantation for 12 weeks (b6-d6), reprinted with permission.

the printing process, some of the designed pores may become closed or densified. Consequently, the porosity, pore size and the strut thickness of the printed implants may undergo slight changes [47] In other cases, with improper printing parameters, the raw materials may unintendional accumulate on the edges of the print cells, and cracks can also be found, resulting in the change of mechanical behavior [48–50]. To address this issue, higher laser or electon beam energy density, finer focusing spot and optimized printing parameters can be employed to fabricate implants with improved dimensional accuracy and surface morphology [51].

2.2.2. *Topological optimization*

Structure and geometry design are key factors in meeting clinic requirements for the 3D printed scaffolds. Due to the fact that pore shape, pore size and porosity may apparently affect the mechanical behavior, biocompatibility of the scaffolds, topological optimization is an effective method for identifying an optimal structure in comparison to traditional design techniques [38]. Up to now, numerous mathematical methods and CAD software have been used to design the optimal structures of porous scaffolds for orthopedic implants, with consideration given to mechanical properties and biocompatibility [52–54]. Although traditional dense metallic orthopedic implants have been widely accepted in clinic applications, the mismatch in mechanical properties between the implants and natural bones is prone to induce stress shielding, which may cause bone resorption and even implant failure [55]. Young's modulus and compressive strength are considered to be the most significant characteristics for orthopedic implants [56]. In comparison to dense metallic implants, 3D-printed porous implants have demonstrated promising adaptability to the mechanical properties of natural bones [57,58].

Structure design plays a critical role in determining the pore size, strut size, and porosity of 3D printed implants, allowing for customization of the mechanical behavior of the implants. Building units with regular cubic, pyramid, and polyhedral structures have been extensively studied for this purpose. Fig. 4a-c illustrated a series of building unit cells design for 3D printed porous implants. Bael et al. [59] systematically evaluated the effect of pore geometry on the SLM Ti6Al4V bone scaffolds. They fabricated six different types of scaffolds with distinct unit cells. The unit cells were designed into triangular, hexagonal and rectangular shape with pore size ranging from 500 to 1000 μm. Compression test showed that scaffolds with hexagonal unit cells exhibited the highest compression stiffness, with stiffness decreasing significantly as pore size increased from 500 μm to 1000 μm. Wang et al. [60] evaluated the influence of pore shape and distribution on the mechanical properties of Ti6Al4V scaffolds. All the four scaffolds in their study had an average pore size and strut size of 500 μm and 400 μm, respectively, with an average porosity and permeability of 70% and 100%, respectively. Under a vertical loading of 100 N, scaffold (Ti-r) with regular distribution of diamond crystal lattice cells showed significantly lower equivalent stress peak and elastic strain, however, the max force that the scaffolds can bear and the Young's modulus were higher for Ti-r scaffolds. Scaffolds with a regular distribution of diamond crystal lattice cells demonstrated better performance than other scaffold designs in terms of mechanical behavior and suitability for clinic applications.

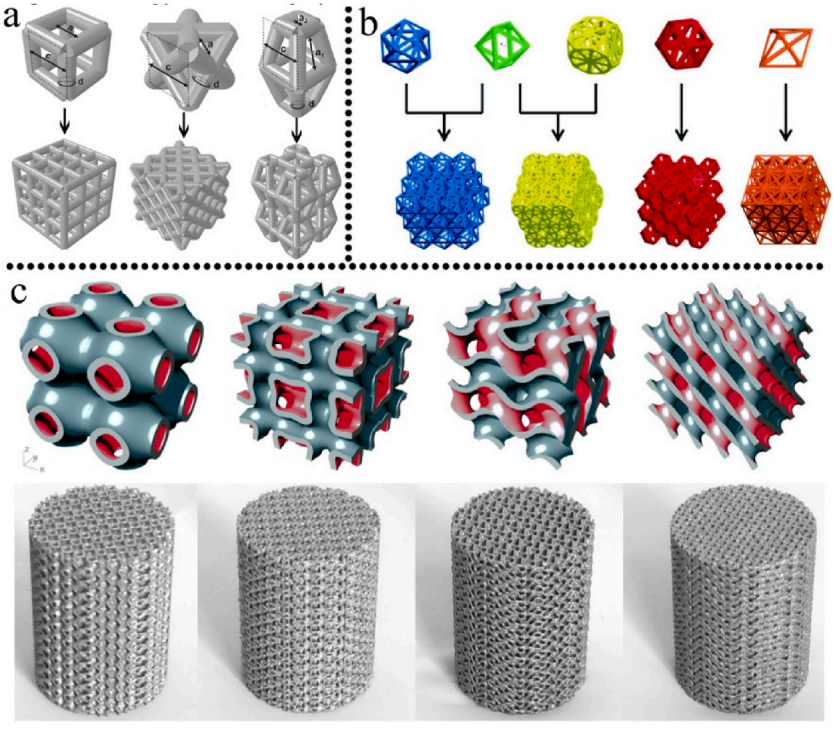

Fig. 4. A series of building unit cells for 3D printed implants. a: from left to right, cubic structure, diagonally orientated struts and modified truncated pyramid [61]; b: examples of five polyhedral units [62]; c: triply periodic minimal surfaces (TPMS) porous units, the bottom rows are resultant blocks or printed scaffolds [63], reprinted with permission.

In order to better imitate the hierarchical structures of native bones, 3D printed porous scaffolds with spatially varying porosity, pore size, or stiffness are particularly desirable [64]. It have been reported that successful implants should compose pore gradient to support the regeneration of natural bones [65–70]. Various solutions have been proposed for fabricating implants with gradient structures, such as changing the types and dimensions of printing unit cells. However, the easiest way is to change the thickness of the struts either in the axial (Fig. 5a,c,e) or radial directions (Fig. 5b,d,f), as shown in Fig. 5. Gradient scaffolds not only stimulate new bone penetration but also minimize the stress shielding effect after implantation [71,72]. To optimize elastic properties and simulate the structures of trabecular bone, Surmeneva et al. [73] developed model structures with layered regular unit cells. The triple- and double-layered porous Ti6Al4V based scaffolds with different pore size for inner and outer holes were successfully printed. The gradient porosity can be ranged from 21 to 65%, while compressive plastic strain and elastic modulus can be tailored from 31 to 212 MPa and 0.9–3.6 GPa, respectively.

Han et al. [74] manufactured continuous functionally graded porous scaffolds based on Schwartz diamond unit cell by SLM. The pore size increased continuously from the distal layer to the proximal layer. By adjusting the graded volume fraction, the elastic modulus and yield strength can be customized within the range of 0.28–0.59 GPa and 3.79–17.75 MPa, which were close to those of cancellous bones. Nune et al. [75] printed interconnected porous functionally gradient Ti6Al4V mesh structure with pore size of 200, 400 and 600 μm by EBM (Electron Beam Melting) and investigated the response of osteoblasts. Their results demonstrated that the expression of actin and vinculin were higher in Ti6Al4V mesh with 200 μm pore size, however, cell nuclei decreased from 600 μm pore

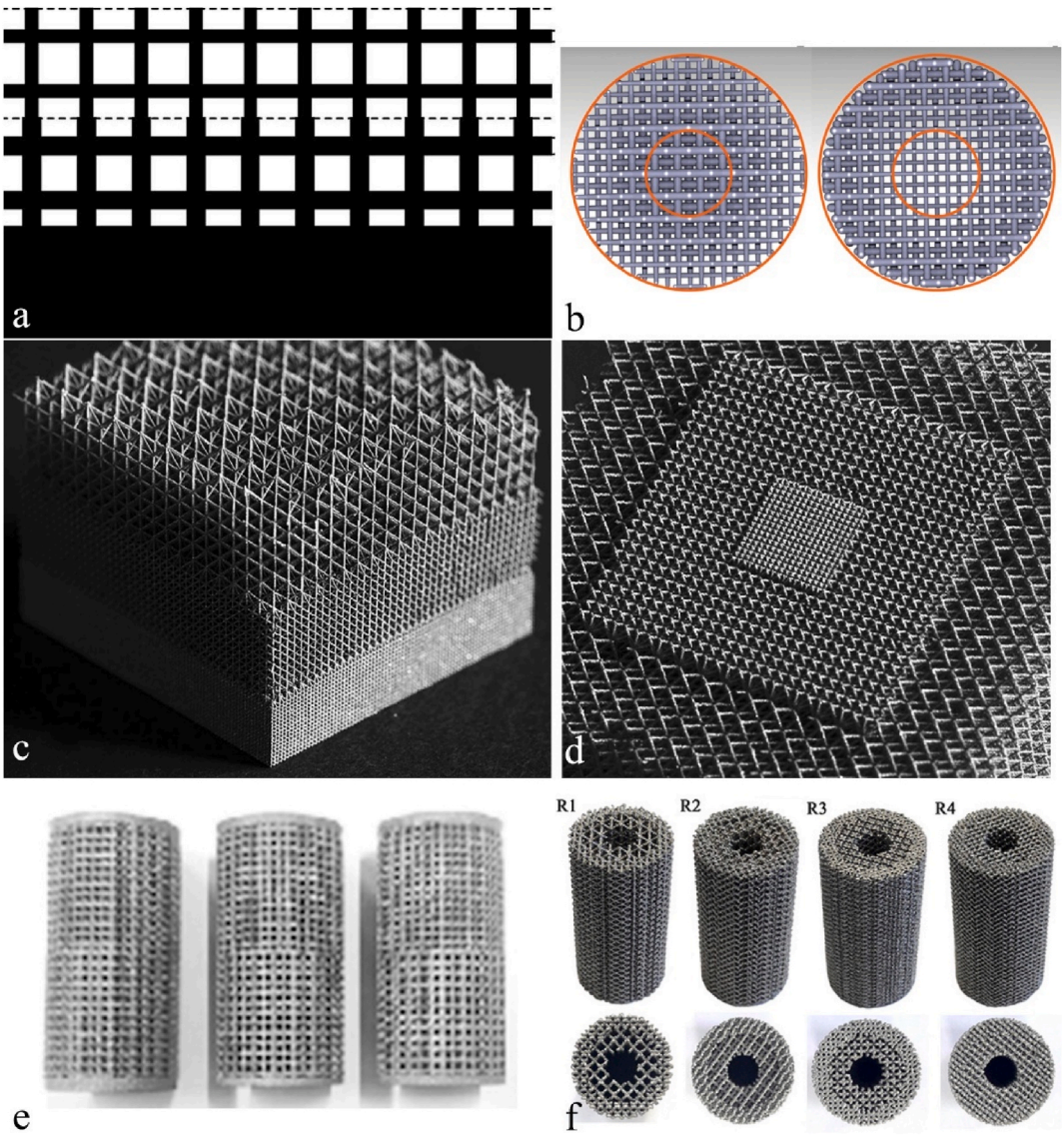

Fig. 5. Porous 3D printed components with gradient structure design. Gradual changes in porosity in the vertical direction (a [83], c [84], e [85]) and in the diagonal directions (b [86], d [84], f [73]), reprinted with permission.

size to 200 μm pore size. After 14 days of incubation, the mesh structure was covered with a thin sheet of cells. The mesh struts were wrapped by cells and the pores were bridged with their filopodia. Compared to larger pore size areas, a number of porous areas where the confluent layer was partially present were observed. They concluded that the gradient mesh structure can be a potential route to minimize mechanical mismatch between bone and Ti-based implants.

In recent years, triply periodic minimal surface (TPMS) has become a popular choice in AM due to its ability to provide various porous structures [76]. TPMS is described by the parametric equation and exhibits high surface area and uniform stress distribution under load-bearing conditions. The structure's shape, porosity, and pore size can be precisely modified by altering characteristic parameters in the function expressions, making it possible to fulfil diverse mechanical requirements in different orthopedic applications [77,78]. There are various TPMS configurations available, such as Primitive, I-Wrapped Package (I-WP), Gyroid, Neovius and Diamond. It has been reported that the Gyroid structure possesses a higher fatigue life and permeability [79,80]. Meanwhile, the I-WP and Neovius structures exhibit higher uniaxial compressive modulus, compressive strength, and energy absorption than Primitive structure [76,81].However, Viet et al. reported that the I-WP structure demonstrated the highest effective yield strength for a given porosity level [82].

2.2.3. *Postprocessing*

For metal 3D printed implants, metal powder particles may undergo partial re-melting, resulting in an undesired rough surface (Fig. 6b). This rough surface, along with internal defects and insufficient layer bonding, may serve as the crack initiation site when under load-bearing conditions if no further processing procedure is performed [87]. Additionally, residual stress may be caused by thermal fluctuations during the printing process [88], which can lead to decreased fatigue behavior of the implants under fatigue loading [89–91]. Since the implant surface serves as a bridge between the implants and surrounding cells and tissues, their interactions are crucial for better clinic outcomes. Therefore, postprocessing would be necessary to achieve better mechanical properties and biological performance for the 3D printed implants.

Post-processing typically involves removing the supporting part, if necessary, as the first step. Subsequently, grinding or machining polishing can be applied to obtain a smoother surface, as depicted in Fig. 6a [92]. In order to further improve the in vitro and in vivo behavior of the implants, heat treatment can be applied. Heat treatment eliminates the surface defects and improves the surface hydrophilic. Consequently, the early cell attachment, proliferation and osteogenesis differentiation can be promoted [93]. Additionally, the heat treatment process can eliminate residual stress and consolidate the implants, thereby increasing their ductility, strength, and fatigue resistance [94,95]. With further processing using hot isostatic press (HIP) processing and surface polishing, the fatigue life of SLM printed Ti6Al4V components can be one or two orders of magnitude higher than of as-printed and wrought Ti6Al4V components [96–98]. Due to the rapid melting and solidification rates during 3D printing process, the existence of non-equilibrium phases can impair the corrosion resistance property of the Ti-based implants. And proper post-heat treatment can decrease the corrosion rate and eliminate pitting corrosion by transforming non-equilibrium phases into equilibrium α and β phases [99].

Recent research has highlighted the importance of surface roughness in promoting osteointegration and bone regeneration in 3D printed scaffolds [101,102]. Surface roughness has been found to not only impact osteoblast adhesion on the scaffolds [103], but also alter cell morphology and osteoblastic differentiation [104]. In preparing heat-treated Ti6Al4V scaffolds, Li et al. [105] demonstrated that increasing the heating temperature resulted in higher surface roughness (Ra = 7.55 ± 0.83 nm, Rq = 9.46 ± 0.92 nm), which improved cell adhesion, proliferation, and bone ingrowth. Other study has shown that cellular proliferation increases when surface roughness is increased from 0.16 μm to 2.19 μm [38]. Ponader et al. [106] reported that cell viability significantly decreased when Ra was higher than 56.9 μm. However, the osteogenic differentiation marker expression did not differ more than twofold for different Ra. The underlying mechanism has been discussed, with the Wnt5A pathway being implicated in osteoblast response to surface roughness, and integrin α2β1 being regarded as responsible for osteoblast response to surface microtopography [107,108]. Except for cell interaction, the roughness of the surface can also act as a collection site for mineral nucleation, such as calcium phosphate precipitation and HA [109,110]. In order to achieve better biocompatibility, other surface modification techniques such as microarc oxidation and surface coating have also been applied to 3D printed scaffolds [111–115].

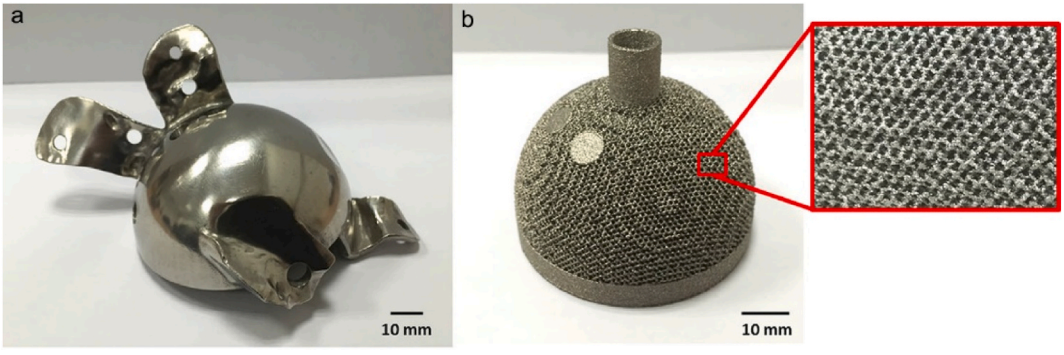

Fig. 6. Surface morphology of: (a) hip joint printed by SLM after polishing and (b) as -printed acetabular cup printed by EBM without any further processing [100], reprinted with permission.

3. 3D printing for orthopedic implants

In addition to its use in anatomy education and surgical planning, 3D printed implants have become increasingly prevalent in bone replacement and fixation. The advantages of these implants, such as customized design and precision control make them superior to conventional implants [116]. The trend towards individualized treatment approaches in modern medicine has led to the widespread acceptance and utilization of customized 3D printed orthopedic implants in patient-specific prostheses [117]. As a result, the number of clinical trials involving 3D printed implantable medical devices has significantly increased in recent years.

3.1. Maxillofacial and oral application

Due to the inherent complex anatomy structure, craniomaxillofacial regeneration or fixation is difficult especially with irregular defects when seldom available implants were suitable for all patients [118,119]. There is a great need for the fabrication of patient-specific craniomaxillofacial implants for clinical use that are both cost-effective and can be produced quickly [120]. For the early applications of scaffolds in maxillofacial bone tissue engineering, polymer [121], calcium phosphate [122–124] and bioglass [122,125] were selected due to their osteoconductive property. However, these scaffolds were lack of load-bearing capacity as they were fabricated as cements, or pastes [126]. Fernandes et al. [127] reported the first 3D printed implants which was employed as a

Table 1
A brief summary of the 3D printed implants in maxillofacial and oral applications.

Clinic cases	Prosthesis Type	Material	Printing techniques	Outcome	Country/ year	Ref
Asymmetric face, collapse of the right face, masticatory problems, malocclusion, and TMJ clicks after mandibular outer cortex split ostectomy (MOCSO)	Titanium mandibular mesh	Titanium	/	Perfect fit the position; correction of facial asymmetry; decreased mouth-opening deviation; disappearance of TMJ pain	China/ 2012	[136]
Complex reconstruction of the craniomaxillofacial area	Titanium plate	Titanium	SLS	Well fitted; individual aesthetic well maintained; no implant-related complications	Germany/ 2017	[137]
Anterior maxillary region injury with loss of upper front teeth along with bone	Implant model for visual inspection and Basal Osseointegrated implant	PLA for model and Ti64 for implant	FDM for model and SLS for implant	All the dentures functionality and aesthetics were restored to that of a health individual	India/ 2017	[138]
Severe maxillofacial trauma, extensive swelling of maxillofacial area, loss of normal occlusal contacts	Ti6AI4V cellular mesh tray	Ti6Al4V	SLM	Discharged at the 3rd postoperative week, no obvious clinical signs of inflammation, implant partially covered by bone callus	China/ 2017	[139]
Case 1: mandibular corpus ameloblastoma, Case 2: squamous cell carcinoma	Grade II titanium	Titanium	SLM	Recovery to oral feeding; returned to a normal diet without any need for analgesics; no pain or visible scar	France/ 2017	[140]
Unilateral end-stage TMJ osteoarthrosis	Fossa component: ultrahigh-molecular-weight polyethylene condylar head component: cobalt-chromium-molybdenum alloy mandibular component: 3D printed titanium alloys	Ti6Al4V	/	Wound healed well without serious scars; no prosthesis displacement, breakage or loosening	China/ 2019	[141]
Post-traumatic zygomatic fixation	medial-lateral 3.5 cm orbital floor defect.	Ti6Al4V (Grade 23)	Metal powder bed fusion	Precise restoration and robust anatomical fitting with no issues	UK/2020	[142]
Temporomandibular joint (TMJ) OA/TMJ synovial chondromatosis	Fossa backing/Ti–6Al–4V ramus and Co–Cr–Mo condylar head	Ti6AL4V/	EBM	No prostheses displacement, breakage or loosening, no severe infection, no swelling and scars, VAS for pain or diet and mandibular function reduced, increased maximal interincisal opening (MIO)	China/ 2021	[143]
Recurrent ameloblastoma in the left mandible	patient-specific implant plate	Ti6Al4V (Grade 5)	SLM	Perfect facial symmetry, normal facial expression movements, normal opening and closing movements, good fit positioning of the implants	Syria/ 2021	[144]

facial prosthesis. The patient suffered a complete maxillectomy, rhinectomy, and resection of the upper lip and aspects of the left and right cheeks. After the failure of four zygomatic oncology implants, an anatomically customized Ti6Al4V implant was manufactured by 3D printing. The facial implant was then placed intraoperatively and fixated with 21 cortical screws. After the operation, the patient adapted well to the facial implants and remained tumor-free for half a year. Roos et al. [128] implanted a Ti6Al4V Direct Metal Laser Sintering (DMLS) frame in a patient with a significant midfacial defect after subtotal maxillectomy. Three years after the operation, the patient was satisfied with mastication, deglutition, and had achieved excellent speech. The Ti6Al4V frame was able to reconstruct large midfacial defects in terms of functional and cosmetic results. However, reconstruction of other large orbital defects remains a challenge in clinical applications [129]. It has been reported that orbital fractures that are operated within 48 h after trauma can reduce postsurgical diplopia and improve prognosis [130]. 3D printed orbital plates with variable thickness have provided optimal functional and aesthetic results for delayed reconstruction of large orbital floor defect [131]. For some complex surgeries, 3D printed implants are extremely useful in saving operation time and reducing the risk of complications and patient morbidity [132–135]. A brief summary of 3D printed implants in maxillofacial and oral applications is shown in Table 1.

3.2. Joint application

In the last few decades, conventional orthopedic implants have been widely accepted for joint replacement occasions [145]. However, these implants are in pre-designed geometry and may not be the best choice for all patients with differing joint anatomies. Additionally, some patients with special injuries, such as revision surgery, may require additional extension of the incision or increased bone amount to ensure the stability and matching of the implants. The traditional implants may not meet the clinic requirements in these cases [146]. The mismatch between conventional implants and bone structures may lead to implant failure [147]. 3D printed joint prostheses with patient-specified designs provide an alternative choice for these situations [38].

3.2.1. Shoulder joint

It was doctor Jules-Emile Pean that conducted the first shoulder arthroplasty in 1893 for a patient who suffered from tubercular arthritis. The prosthesis, composed of a rubber head and platinum stem, was removed after two years due to tubercular infection [148]. Over the centuries, shoulder arthroplasty has developed and is now considered the fastest growing procedure among all other orthopedic joint replacements [149]. In clinic situations, shoulder arthroplasty is often a result of tumor resection, and the main goal of shoulder reconstruction is to preserve adequate basic functions for the daily life of patients [150]. Over the past few decades, autograft, allograft, customized, and modular prosthesis have been widely applied in shoulder arthroplasty. However, there is still a need for optimal implants [151]. Although 3D printed total shoulder prostheses are not yet available, other 3D printed implants such as glenoids, clavicles and scapulas have been reported [146,152]. Instead of wide resection of the middle third of the clavicle followed by autologous bone graft reconstruction and radiotherapy in a male patient who suffered from langerhans cell histiocytosis (LCH) on his left shoulder, Diego et al. [153] printed a porous titanium pseudo-prosthesis to accomplish clavicular reconstruction after tumor resection. No pain on palpation or mobilization were occurred with complete range of motion of the left shoulder at 3 months after operation. 2 years after operation, the left shoulder recovered normal function without any limitation. The authors concluded that the 3D printed titanium pseudo-prosthesis allow for full resection of the oncological margins, without the need for local radiotherapy or systemic chemotherapy for the patient. Daniel et al. [154] successfully implanted a 3D printed glenoid implant into a 56-year-old woman who had suffered a severe glenoid defect 12 years after total shoulder replacement, resulting in almost total destruction of the glenoid. The immediate postoperative X-ray images indicated that the implant was successfully implanted in the right position. Only six weeks after the surgery, the patient was able to resume household activities. Her constant score improved to 51 points after 2.5

Table 2
A brief summary of the 3D printed implants in shoulder joints applications.

Clinic cases	Prosthesis Type	Material	Printing techniques	Outcome	Country/ year	Ref
Case 1: clavicle ES, case 2: right scapular ES	porous clavicle prosthesis and porous scapular prosthesis	Ti6Al4V	EBM	Proper placement of implant. No neurovascular bundle injury. No local recurrence or metastasis. Shoulder motion recovery	China/ 2015	[152]
Case 1: extraskeletal ES; case 2: subscapularis muscle synovial sarcoma	porous scapular prosthesis	Titanium	/	No neurovascular bundle injury or other complications. No local recurrence or metastasis. No implant breakage and joint collapse.	Italy/ 2018	[150]
Revision of total shoulder arthroplasty (TSA) with severe bone defects	macro-porous shoulder prosthesis	Ti6Al4V	EBM	Anatomically satisfying reconstruction, accurate prosthesis placement, improved shoulder function for daily activities and increased quality of life.	China/ 2018	[156]
Primary malignancies in the proximal humerus underwent intra-articular *en bloc* resection	proximal humeral prosthesis with glenoid component and intermediate segment	Ti6Al4V	EBM	No aseptic loosening, breakage, fracture, or infection, but two cases experienced detachment of the taper. Tight osseointegration at the bone-prosthesis interface. New bone formation in porous structure	China/ 2022	[157]

years of follow-up. According to Fan et al. [152], three porous Ti–6Al–4V prosthesis manufactured via EBM have been applied in shoulder joints reconstruction. A 21-year-old woman with clavicle Ewing's sarcoma (ES) was diagnosed with a large expandable osteolytic lesion affecting the entire clavicle. The printed prosthesis not only matched the excised clavicle well but also reduced the modulus of the implant. Proper placement and clavicular symmetry were evident in X-ray images taken 2 years after the surgery. A size-matched scapula prosthesis was implanted in 35-year-old woman who diagnosed with right scapular ES. The major blood vessels and nerves to the upper extremity were preserved. After 21 months of implantation, proper articulation of the scapular prosthesis was observed. Beltrami et al. [150] reported on two patients who received 3D printed custom-made porous Ti scapular prostheses. Twenty and sixteen months after operation, respectively, no local recurrence or metastasis was found, and motion scores for the shoulder were 87% and 63%, respectively. No implant breakage or joint collapse occurred. Another 3D printed honeycombed titanium segmental scapula prosthesis was also applied in the reconstruction of an irregular bony defect following limb salvage surgery for chondrosarcoma tumor resection [155]. At the 28-month follow-up, the prosthesis was in good position with no tumor recurrence. At the final 32-month follow-up, the patient was also in good condition with no discomfort in the surgically treated shoulder. A brief summary of the 3D printed implants applied in shoulder joints reconstruction application is shown in Table 2.

3.2.2. *Wrist joint*

Severe injury or tumor resection of the wrist often requires either arthrodesis or arthroplasty to restore the function of the wrist [158]. Therefore, wrist replacement surgeries have been increasing. Although previous wrist prostheses were claimed to be suitable for clinic application with preserving basic joint functions [159–162], implants failure ascribed to prosthesis loosening, dislocation, or infections may compromise clinic outcomes [162]. Nowadays, 3D printing techniques are able to produce upper limb orthoses utilized for fixation or regeneration of the wrist to support injured limbs [163]. Lu et al. [164] proposed a custom-made 3D printed prosthesis with a best-fit articular surface for wrist joint arthrodesis after giant cell tumor resection. During 2015 and 2017, they conducted eleven implantations for giant cell tumor patients. Prior to their operation, all patients claimed painful, after the operation, seven patients reported no pain, while four other patients continued to suffer from moderate pain. The range of motion was significantly improved after the operation and the grip strength also increased from 17 mmHg to 23.6 mmHg. During the two years follow-up, no deaths, tumor recurrences, metastases, or amputations were observed. In terms of the implanted prosthesis, no aseptic loosening, subluxation, or breakage were found. They suggested that 3D-printed prosthetic reconstruction can be a suitable alternative option for recurrent distal radius tumor resection. In cases of large structural defects after tumor resection at the distal end of the right radius, a 3D printed tantalum implant was applied to preserve the normal appearance and function of the wrist. 24 months after the operation, only slight pain was occasionally occurred, and no local recurrence or metastasis was found. However, slight bone resorption between the tantalum prosthesis and radius was observed according to CT results [165]. Xie et al. employed mirror technology and data registration technology to design and print a lunate prosthesis for a 41-year-old patient with lunate collapse [166]. After implanting the 3D printed lunate prosthesis in its original anatomic position, the wrist was fixed with plaster for 4 weeks. 12 months after surgery, the patient was able to use the wrist in sports activities with mild pain, and no weakness or numbness were observed. Additionally, during the last evaluation, the wrist exhibited nearly full range of motion and grasp force. Xu et al. [167] claimed to have conducted the first comprehensive clinical guide for the application of 3D printed prostheses. They designed and manufactured a novel 3D printed prosthetic hand for a child who suffered a severe acute mangled injury of right hand after a mincing machine accident. 4 weeks after surgery, the wound had healed successfully, and stitches were removed. After personalized prosthetic training and rehabilitation program, the child's parents were satisfied with the prosthesis. The child was able to complete various daily activities such as eating, writing, self-dressing, and even riding a bike with the prosthesis. A brief summary of the 3D printed implants in wrist joints applications is shown in Table 3.

Table 3
A brief summary of the 3D printed implants in wrist joints applications.

Clinic cases	Prosthesis Type	Material	Printing techniques	Outcome	Country/ year	Ref
Lunate density was uneven and the height and width of lunate were collapsed	lunate prosthesis	/	/	Able to use wrist with mild pain during sport activities after 12 months. No weakness and numbness. Nearly full range of motion and grasp force. No degenerative arthritis and prosthetic dislocation. Prosthesis placed in original anatomic position	China/ 2018	[166]
Distal radius giant cell tumor (GCT)	uncemented shaft and stem coated with HA	Titanium	EBM	No tumor recurrence, metastasis or amputation. No degenerative changes or complications. Reliefed from pain. Improvement in ROM and Mayo wrist score, decrese in DASH score.	China/ 2018	[168]
Lunate replacement arthroplasty with Kienböck's Disease in Different Stages	3D printed lunate prosthesis	Ti6Al4V	EBM	No prosthesis dislocation or subluxation. Significantly increment in extension range and flexion range. No incision infections, cysts, or synovitis in the radial or carpal bones.	China/ 2020	[169]
Osteosarcoma of distal radius	3D printed porous tantalum prosthesis	Tantalum	/	Fast recovery with occasional slight pain. No local recurrence and lung metastasis, slight bone resorption between prosthesis and radius 24 months after operation	China/ 2021	[165]

3.2.3. Hip joint

Osteoporosis related hip fracture is one of the most common public health issue, especially for elder individuals. Other hip fracture caused by trauma can result in hip dislocation or acetabular facture. In such situations, hip arthroplasty is commonly applied to restore hip function [170–173]. Due to their superior mechanical properties and biocompatibility, Ti and its alloys have been used in hip arthroplasty for many years. However, such Ti-based prostheses are in a fixed shape and additional adjustment is required before implantation. Hence, in emergency situations, this can waste valuable time and may also create additional risks for patients [174,175]. Over the years, new manufacturing techniques such as 3D printing have been applied to total joint arthroplasty [176]. In a 2-year follow-up study, Wang et al. [177] compared conventional hip replacement with 3D printed replacement in a total of 74 patients who had severe hip deformiies. For the 3D printing group ($n = 17$), patients exhibited a shorter time (1.5 ± 0.2 vs 2.1 ± 0.3 days, $p < 0.001$) to postoperative weight bearing. Meanwhile, the postoperative Harris hip scores (HHS, 93.5 ± 3.2 vs 91.4 ± 2.9, $p = 0.013$) were higher than the conventional group. However, in terms of postoperative infection and prosthesis loosening, the 3D printing group also exhibited significantly higher infection ($n = 4$ vs $n = 2$) and loosening ($n = 4$ vs $n = 1$) rates. They believed the 3D printed prosthesis with tailored high precision may be a good solution to improve operation success rates of complex and difficult surgeries. They also stated that more cases should be conducted in the future to evaluate their effectiveness and safety. Nine more patients were reported to have received total hip arthroplasty (THA) with a 3D printed custom acetabular component to correct extensive acetabular defects, with an average follow-up time of 28.8 months [178]. The final implants were matched to the patients' individual anatomy. The overall implant-associated survival rate was about 88.9%, with only one patient requiring revision surgery due to implant failure after 13 months. The HHS increased significantly from 22.1 at admission to 58.7. Nonetheless, the authors believed that the manufacturing process should be faster as the present custom prosthesis takes several weeks to complete. Baauw et al. [179] reported a similar clinical trial where 12 patients with failed acetabular reconstruction and large bone defects were recruited. Although four patients had complications, there were no infections or need for additional surgery. All the patients were satisfied with the custom-made implant and daily functioning was improved in most patients. While for a patient who suffered from periprosthetic joint infection (PJI) and femoral defect after THA, a 3D printed antibiotic spacer was initially placed, followed by PJI debridement. Then, a 3D printed proximal femur prosthesis (PFP) was applied to reconstruct the large, atypical segmental femoral bone defect after the PJI was eliminated. 20 months after the surgery, no infection recurrence and prosthetic loosening can be found. The 3D printed PFP exhibited near-perfect anatomical reconstruction of the hip with a near-normal range of hip movement [180]. A brief summary of the 3D printed implants in hip joints applications is shown in Table 4.

3.2.4. Knee joint

As the load-bearing joint, the knee is highly susceptible to osteoarthritis (OA) or trauma. Total knee arthroplasty (TKA) has been widely accepted as the most useful solution in treating end-stage osteoarthritis worldwide [182]. With increasing aging problems in developed countries, TKA is rapidly becoming more prevalent [183,184]. Although TKA is a reliable surgery with implant revision rates about 5% at years, prosthesis loosening, dislocation and instability still need to be resolved [185,186] and nearly 19% of patients remain dissatisfied post TKA [187]. Conventional knee prostheses may not be appropriate for patients with severe bone defects in the distal femoral or proximal tibia, and large bone loss also limites the use of standard knee prostheses [188]. As TKA plays a vital role in knee replacement, improving the long-term outcomes of knee implants is necessary for both surgeons and engineers. Porous structured 3D printed knee prostheses seem to be a new candidate for TKA [38,189,190]. It has been reported that the initial mechanical stability of the 3D printed porous Ti revision metaphyseal cone implants was either equivalent or better than conventional tantalum cones, as measured by micromotion under physical loading situations [191]. Patient-specific 3D printed cones for revision TKA can be easily placed in the defect after minimal adaption of the host bone with no technical difficulties, thus facilitating the surgical procedure [192]. In the case of unicondylar femoral defects reconstruction caused pathological fractures induced by GCTs, the use of 3D printed custom-made prostheses not only reduces blood loss but also shortens operation time. In terms of Musculoskeletal Tumor Society (MSTS) scores and range of motion of the knee, the 3D printed group perform much better than the total knee replacement (TKR) group [193]. Ma et al. [194] implanted 3D printed personalized Ti plates in 12 patients (7 cases of osteosarcomas, 3 cases of GCTs, 1 case of ES and 1 case of chondrosarcoma after microwave ablation of tumors around the knee. The customized plates were matched well with

Table 4
A brief summary of the 3D printed implants in hip joints applications.

Clinic cases	Prosthesis Type	Material	Printing techniques	Outcome	Country/ year	Ref
Severe hip deformity caused by either hip tuberculosis (TB) or developmental dysplasia of the hip (DDH)	3D printing hip arthroplasties	Titanium	EBM	Shortened time to postoperative weight bearing. Improved postoperative HHS	China/ 2017	[177]
Total hip arthroplasty	3D printed acetabular cup with a porosity of 50%–80%, pore size of 600–800 μm	Titanium	EBM	No prosthesis related complications. Improved average HHS. New bone formation in the porous cup.	China/ 2021	[181]
Chronic periprosthetic joint infections (PJI) and segmental femoral defect	3D printed personalized proximal femur prosthesis	/	/	Significantly improvement in HHS, no sign of implant loosening, significant symptomatic improvement with a near-anatomical hip joint	China/ 2021	[180]

the bone surface. Knee gait analysis revealed that all the patients had good status for knee functions during their daily activity. They also suggested that the design of several small holes on the distal plates allowed the maximum retention of the knee joint, due to the mechanical construction. 3D printed porous implants combined with bone grafting in subchondral GCT of the proximal tibia was also reported [195]. The personized porous implant is utilized to mechanically support the graft and subchondral area. The VAS score decreased from 7 to 0 after surgery. At 29 months after surgery, knee motion was within a normal range with no detectable difference. Furthermore, no degenerative, fracture or collapse was found. The shape and thickness of the porous plate, strut length, pore size and porosity are the main factors in achieving superior clinic outcomes. A brief summary of the 3D printed implants in knee joints applications was shown in Table 5.

3.2.5. Feet and ankle joints

Total ankle replacement (TAR) has been approved for clinical applications in treating ankle related injuries, but satisfactory clinical outcomes have been difficult to achieve compared to other joints [199,200]. Due to the limitation of treatment options, ankle arthritis, avascular osteonecrosis, and osteomyelitis remain a surgical challenge in foot and ankle treatment [201–205]. Furthermore, the compact size of ankle joints and the higher resultant moment and compressive force they experience make it complicated to develop ankle replacements [200]. Consequently, ankle replacement has received less attention from clinical and industrial sectors, and only a small number of sizes are currently available [206]. The irregular morphology of the ankle joint further complicates the development of traditional plates, which may not match the bone surface [207]. Recent studies have shown that patient-specific designs of ankle prostheses are expected to achieve better results in TAR [208–211]. In an ankle osteoarticular infection patient who requring pain relief and ankle fusion, the 3D printed titanium talus was superior than proximal trabecular tibial cone [212]. In order to improve the clinical performance of 3D printed plates for foot and ankle joints fusing, finite element analysis (FEA) can be applied to optimize the stress distribution of the implants [207].Wardhani et al. [200] analyzed 3D printed ankle implant models (both solid and porous structure) and the effects of ankle postures on the biomechanical performance of the implants via FEA. The study found that implant models with a flat tibial component shape exhibited lower tibial bone stress when compared to the curved or tilted shapes, while tibial component shape had little influence on talus bone stress. The implant models with a medium pore size (0.8 mm in width and 1.0 mm in depth) had lower talar component stress. Dekker et al. [213] conducted a retrospective study on patients who underwent tibia, ankle, or hindfoot reconstruction with a patient-specific 3D printed Ti prosthesis by a single surgeon. Of the 15 patients, 13 were successfully implanted with the 3D printed prosthesis. One failure was due to deep infection, and the other due to nonunion at ankle arthrodesis. American Orthopedic Foot and Ankle Score (AOFAS) improved from 28.4 to 64.8, and the Foot and Ankle Ability Measure Activities of Daily Living score (FAAM ADL) also increased from 23.5 to 62.8. Meanwhile, the 100-mm VAS pain scores significantly decreased from 89.0 to 23.9. Belvedere et al. [209] claimed to have fabricated and tested a custom-made total ankle prosthesis for joint arthritis using 3D printing for the first time. They also proposed a comprehensive procedure for custom-made total ankle replacement. After implantation in cadaver specimens, physiological motion was well restored, and load-displacement curves exhibited that joint stability was also well restored by the custom-made artificial joint. Hamid et al. [214] successfully implanted a Ti6Al4V prosthesis in a woman who sustained a left open distal intra-articular tibia fracture with substantial distal tibia bone loss. 6 months later, the patient could walk on her feet all day without any ambulatory aids. Heel pain at the nail insertion site appeared at 13 months after

Table 5
A brief summary of the 3D printed implants in knee joints applications.

Clinic cases	Prosthesis Type	Material	Printing techniques	Outcome	Country/ year	Ref
Campanacci Grade II GCT with no pulmonary metastasis	3D printing porous implants with porous plate and shrut to mechanically support the graft and subchondral area	/	/	VAS score decreased to 0. Normal range of knee motion reached. No degenerative changes, no fracture or collapse. No local recurrence or lung metastasis.	China/ 2019	[195]
Revision total knee arthroplasty	3D printed patient-specific metaphyseal and diaphyseal cones	Titanium powder	/	No technical difficulties in positioning and implanting the cones. No indications for revision surgery. No complications. Significantly improvement of Knee Society Score, Western Ontario and McMaster Universities Osteoarthritis Index and Forgotten Joint Score. Osteointegration achieved within the first 6 month after surgery.	Russian/ 2021	[196]
Joint-preserving prosthetic reconstruction after low-grade osteosarcoma excision	3D printed tibial plate coated with hydroxyapatite	Ti6AL4V (ISO 5832-3)	/	Good alignment and no implant loosening. The patient can walk independently without aid or pain 10 month after surgery. No tumor recurrence. The range of motion for the affected knee reached 100°.	Turkey/ 2021	[197]
Giant cell tumor in proximal tibia	a porous truncated ellipsoid cone-shaped plate and a porous square frustum-shaped strut	titanium alloy	EBM	No surgical-related complications. No degeneration of the knee joint. No aseptic loosening or breakage. Improved Musculoskeletal Tumor Rating Scale and VAS decreased.	China/ 2021	[198]

implantation but resolved two months later. Bone penetration into the talus, calcaneus and 3 of 4 cortices of the tibia were proved by CT scanning at 13 months after implantation. A brief summary of the 3D printed implants in feet and ankle applications is shown in Table 6.

3.3. Spine application

The incidence of spinal related diseases, such as degenerative disc, spinal deformities, tumors, and other injuries, is on the rise. To meet the clinical requirements, a lot of different spinal implants and devices have been designed and fabricated to accelerate fusion, restore deformity, provide fixation, and reconstruction or strength the spine [216]. Due to the complex anatomy structure of the spine, spinal surgery is a complicated and risky procedure. However, in vivo animal models have demonstrated the feasibility of 3D printed prosthesis in spine applications [217]. Recently, several reports have suggested that 3D printed spinal implants can yield better clinical results for complex spinal surgeries [210,218–221]. Notably, tt was professor Zhongjun Liu and his team who all came from China

Table 6
A brief summary of the 3D printed implants in feet and ankle applications.

Clinic cases	Prosthesis Type	Material	Printing techniques	Outcome	Country/ year	Ref
Left open distal intra-articular tibia fracture with substantial distal tibia bone loss	custom 3D printed scaffold with patented truss structure	Ti6Al4V	/	By 6 months, the patient returned to work without ambulatory aids and with regular shoe wear. 15 months after surgery, the VAS for pain is 0. 13 months, a focal area of no radiographically identifiable bony bridge at the proximal anterior junction of the residual tibia and the custom implant	USA/ 2016	[214]
Mesenchymal sarcoma of the talus	total talar prosthesis with upper modular component made of ultra-high molecular weight polyethylene (UHMWPE) for articulation with the tibia and fibula, and lower component made of 3D printed titanium alloy for articulation with the calcaneum and navicular	Titanium alloy	/	Patient was disease free 6 months after surgery, walk almost normally without any aid or pain. Roentgenograph showed that the prosthesis and the screws were in stable position, and no abnormalities	China/ 2018	[205]
Foot drop	3D printed personalized plate	Ti6Al4V powders	EBM	Short operation time and minimal blood loss. No infection or fracture of the internal plate. Well-matched to the bone surface. Significant improvement in AOFAS and Short-Form 36 (SF-36) scores 36 months after surgery.	China/ 2021	[207]
Talar necrosis and collapse (TNC)	3D printed talar prosthesis with porous talonavicular and subtalar articular structures and screw fixation channel	Titanium alloy powder	EBM	No degenerative arthritis and prosthetic dislocation. The talar arc length, talar height, talar width, tibiotalar alignment angle, talar tilt angle, Bohler's angle, Meary's angle were all improved. Satisfaction with the implantation, normal activities can be done one month after operation.	China/ 2021	[215]
Osteoarticular infection of an ankle	titanium talus	Titanium	/	Fusion was achieved 4 months after surgery, function improvement 15 months after surgery, apparent signs of osseointegration, capable of walking without external aids	Spain/ 2021	[212]
Foot drop in both feet	personalized plate (P-Plate) for tibiotalocalcaneal arthrodesis	Ti6Al4V powder	EBM	Plate was well-matched to the bone surface 3 months after surgery. No complications. The gait and AOFAS and SF-36scores improved.	China/ 2021	[207]
Chronic osteoarthritis of left ankle after a failed tibiotalar arthrodesis with an anterior plate. Active fistula on the external region of the ankle	3D printed custom-made talus implants	Titanium	/	Fusion was achieved 4 months after surgery. Obvious functional improvement and partial osteointegration of the implants at a 15 month follow-up. No displacement or rupture.	Spain/ 2022	[212]

implanted the first personalized 3D printed porous Ti-based vertebral body into a patient to reconstruction the upper cervical spine in the world [222]. To facilitate bone infiltration, both the pore size and shape of the implant were carefully designed based on their previous studies [223]. One year after surgery, implant osseointegration was confirmed by the newly formed bone in the built-in vertical slit in the center, and no subsidence or displacement of the implant was observed. Lumbar interbody fusion is a common case in spinal surgery. Zhang et al. [224] conducted a study to evaluate the biomechanical performance of transforaminal lumbar interbody fusion with 3D printed PEEK and Ti6Al4V cages. Both PEEK and fully porous Ti6Al4V cages reduced the maximum stresses in the cage and endplate in all motion modes compared to the solid and partially porous cages. Moreover, when compared to PEEK cages, fully porous Ti6Al4V cages not only reduced stress but also increased the range of motion. The authors suggested that fully porous Ti6Al4V cages with a porosity between 65% and 80% would be a better choice than conventional solid PEEK cages. Similar results had also been reported by Tsai et al. [225]. They suggested that porous 3D printed cages with a pillar diameter of 0.4 mm, a pillar angle of 40°, and a porosity between 69% and 80% exhibited better mechanical behavior. Spetzger et al. [226] reported the implantation of an individualized cervical Ti cage for cervical fusion. The cage was fabricated with a porosity and pore size of 80% and

Table 7
A brief summary of the 3D printed implants in spine applications.

Clinic cases	Prosthesis Type	Material	Printing techniques	Outcome	Country/ year	Ref
C2 ES, staged as IIB according to the Weinstein-Boriani-Biagini classification, with no metastasis	3D printed self-stabilizing artificial vertebral body (SSAVB)	Titanium alloy	EBM	Implant osseointegration 1 year after surgery, no subsidence or displacement of the construct, no local recurrence of the tumor. Improved neurological function.	China/ 2016	[222]
T9 pseudo-myogenic-hemangioendothelioma, and extension into the paravertebral region and ribs	The custom 3D printed vertebra cage prosthesis with fixation holes for pedicle screws	Titanium	/	Patient returned to full schooling 3 month after surgery, paracetamol was required for release pain, the patient can return to netball and school sports. Implant was well positioned and had integrated with the adjacent end plates 6 months after surgery	Australia/ 2017	[231]
Papillary thyroid carcinoma with very large lytic lesion involving C2–C4 vertebrae	columnar structure Self-stabilizing Artificial Vertebral Body (SSAVB) with bilateral shoulders	Ti6Al4V	/	Quick improvement in neurological function and Japanese Orthopaedic Association (JOA) score. Good cervical vertebrae sequence and implant position at the 12-month follow-up point. The JOA score was 16/17 and the patient can independently engage in daily activities.	China/ 2017	[232]
Complete spinal cord injury below T11 with exacerbated infectious spondylitis, and spine fusion failure and screw loosening	3D printed cages with 4 arms to fix the screws	medical grade Ti6Al4V	EBM	2 weeks after surgery, the back pain became tolerable and ambulation in wheelchair. No further signs of infection, mechanical complication, or newly developed neurologic symptoms. The fusion of the bone around the implants was stable. No loosen of the pedicle screws.	Korea/ 2019	[233]
Renewed symptomatology after anterior cervical discectomy and fusion	porous titanium cages	Ti6Al4V ELI Powder	SLM	The cage revealed white tissue, similar to bone, lamellar bone can be found in the cage surface, the bony tissue infiltrated in the anterior 2/ 3rd of the cage, no fibrous tissue interface between the newly formed bone and the cage struts, no inflammatory cells or tissue reactions	Germany/ 2020	[234]
Posterior vertebral column resection (PVCR) due to Kümmell's Disease complicated by neurological deficits	3D-printed artificial vertebral body (pore size: 800 ± 200 μm, 80% porosity)	Ti6AL4V	EBM	Significantly lower operative duration and blood loss, no implant related complications	China/ 2020	[235]
Cervical spondylotic myelopathy	3D-printed interbody fusion cages	Titanium alloy powder	EBM	No spinal cord injury, esophageal fistula, cerebrospinal fluid leakage, cervical hematoma or wound infection. Improved JOA, cervical curvature index (CCI) and SF-36 score.	China/ 2021	[236]
Reconstruction of cervical lateral mass to maintain cervical stability	3D-printed lateral mass prosthesis	Ti6A14V ELI	EBM	No implant-related complications such as prosthesis loosening, displacement, and compression were observed at the last follow-up	China/ 2022	[237]

0.65 mm, respectively. It can also self-locate into the correct position and impossible to move from the implantation site from any direction after suspending distraction. The superior structure design provided an ideal environment for excellent secondary bony fusion without additional bone graft. In another study, 3D printed patient-specific implants were used for vertebral body replacement (VBR) in cervical spondylotic myelopathy (CSM), with six patients showing excellent clinical outcomes three months following the procedure [227]. 3 months later, all the 6 patients were satisfied with the clinic result and they progressed from Grade II to Grade I or regained normal functions of the neck. During the 3 months' follow-up, the Neck Dysfunction Index (NDI) and VAS scores were all decreased. 3D printed customized prostheses can also help to reconstruct spine functions after tumor resections [228–230]. A brief summary of the 3D printed implants in spine applications is shown in Table 7.

3.4. Pelvic application

Pelvic fracture treatment and reconstruction after pelvic tumor surgery remain challenging issues for surgeons due to the complex and irregular anatomy structures in the region and the presence of important vessels and nerves in the vicinity [238]. This often leads to unsatisfactory clinical outcomes, which can result in high disability or fatality rates [239,240]. Despite the fact that traditional off-the-shelf prostheses have been used for fixation or structural support, the implants and surrounding tissues usually poorly matched, leading to the need for additional adjustment [241]. Furthermore, the use of mismatched prostheses may lead to complications, such as implant loosening [242]. In order to solve these limitations, patient-specified pelvic prostheses have been proposed and developed with 3D printing techniques [243–245]. FEA result revealed that customized Ti6Al4V pelvic prostheses printed via EBM are reliable in terms of mechanical behaviour under the most common daily activity (such as waking, going up stairs or stumbling) [246]. When compared with conventional allograft implants, the individualized 3D printed porous Ti6Al4V prosthesis has exhibited better clinic outcomes in terms of surgery incision length, surgery time, and blood loss for bone defect reconstruction after pelvic tumor resection [247]. Furthermore, the 3D printed patient-specific prosthesis can be navigated to the pre-planned position during reconstruction surgery after pelvic tumor resection with the help of an image-guided surgical navigation system [243]. Wang et al. [248] reported a complete case in which a pelvic prosthesis was designed, printed, and implanted successfully. The pelvic bone plate was successfully implanted with a minimal incision of only about 7 cm, and both the operation duration and bleeding loss were reduced. The pelvic fracture exhibited favorable recovery according to CT scanning. However, the follow-up results were not presented. A 3D printed modular hemipelvic prosthesis for pelvic reconstruction after tumor resection was also reported [249]. After the implantation, the hip joint exhibited good range of motion and stability, with good joint function and HHS improving from 42 to 81. The patient could live

Table 8
A brief summary of the 3D printed implants in pelvic applications.

Clinic cases	Prosthesis Type	Material	Printing techniques	Outcome	Country/ year	Ref
Left-side acetabular fracture	completely-attached, customized, titanium alloy bone plates	Ti6Al4V	SLM	Reduced implant numbers for patients, minimized surgery incision, reduced operation time, well matched with the fracture block	China/ 2016	[248]
Recurrence of chondrosarcoma, loosening of the semi-pelvic prosthesis and a broken screw	pelvic prosthesis with sacrum component and acetabulum component	Ti6Al4V	EBM	Prosthesis in good position, good ROM and stability, HHS increased from 42 preoperatively to 81 postoperatively.	China/ 2018	[249]
Chondroblastic osteosarcoma with no neurological dysfunction	sacral implant	Ti6Al4V medical grade powder	EBM	Visual Analog Scale (VAS) score decreased from 8 immediately after surgery to 3 a year after surgery. No complications observed one year after surgery. Prosthesis well maintained at one year after surgery. Bone ingrowth into the titanium porous structure and bone fusion between medial side of right sacrum	Korea/ 2017	[252]
Bone reconstruction after pelvic tumor resection	reconstruction prosthesis with porous structure	Ti6Al4V	EBM	Better performance in terms of average incision length, duration of surgery, blood loss during operation and MSTS score compared with conventional nail-rod fixation system. No incision infection, no implants loosening or breakage, no tumor recurrence	China/ 2021	[247]
Bony defect reconstruction after pelvic tumor resection	3D-printed anatomically conforming pelvic prosthesis	Ti6Al4V	/	No local recurrence or distant metastases, no sign of hip dislocation, prosthetic loosening, no delayed wound healing or periprosthetic infection.	China/ 2020	[245]
Reconstruction after pelvic bone tumor resection	3D-printed mesh-style titanium spacer/ anatomical plate	Ti6Al4V ELI Powder	EBM	Normal gait with mild or no pain, improved MSTS score	South Korea/ 2021	[253]

independently five months after surgery. Further FEA results suggested that the peak stress at the hemipelvic prosthesis and fixation screws were safe enough. Liang et al. [250] implanted 35 cases of 3D printed Ti alloy pelvic prostheses to reconstruct the pelvic function after different pelvic tumor resections (type I and type I+IV). A higher average MSTS was achieved than with conventional prosthesis [251]. An EBM printed Ti6Al4V pelvic implant was applied in a patient with pelvic chondrosarcoma. After tumor resection, the pelvic implant was fixed to the remaining pelvic and sacrum with screws. 16 months after surgery, the implant was stably fixed in the right position, and no screw loosening or implant breakage were observed [152]. A brief summary of the 3D printed implants in pelvic applications is shown in Table 8.

4. Current challenges and future perspectives of 3D printing in orthopedics

Combined with imaging techniques and FEA remodeling or simulation, 3D printing is now increasingly being adopted in clinical orthopedic applications. Compared to traditional solid implants, 3D printed implants with porous structure not only minimize the stress shielding effect but also promote new bone infiltration and implant stability [254,255]. It is believed that 3D printed implants will bring revolutionary changes to the future orthopedic practice. Although a large number of clinical results have been reported thus far, challenges and perspectives still need to be addressed before extensive clinic trails can be conducted for 3D printed implants, as shown in Fig. 7.

4.1. Current challenges

4.1.1. Raw materials

Currently, the most commonly used raw materials for 3D printed implants are Ti and Ti-based powers. Although, Ti and Ti-based alloys demonstrate good biocompatibility and osteoconductivity, pit corrosion in a physical fluid environment under load-bearing conditions may result in implant failure. Additionally, the mismatch in stiffness and elastic modulus between Ti-based implants and natural bone remains a problem that must be addressed. β-phase Ti alloys with a comparable elastic modulus to bone can be considered as an alternative. By combining with 3D printing techniques, the modulus of high strength (~800 MPa)/low modulus (49 GPa) Ti–24Nb–4Zr–8Sn alloy was significantly reduced to 4.36 GPa, which is close to that of cancellous or trabecular bone [256]. Similar results were also observed for Ti–35Nb–2Ta–3Zr alloy. A 3D printed porous Ti–35Nb–2Ta–3Zr implant with a pore size of 0.48 mm exhibited a modulus of about 3.1 GPa [257].

With shape memory effect (SME), superplasticity (SE), low Young's modulus (40–60 GPa), and good biocompatibility, Nickel-titanium (NiTi) alloys are widely used as orthopedic implants. However, NiTi alloys are inherently reactive and ductile, which makes their fabrication and processing challenging [258]. In comparison to conventional casting or powder metallurgy methods, AM provides a solution to these challenges as it allows for the printing of near-net-shape NiTi implants without requiring additional tooling [259]. By adjusting the ratio of Ni and Ti powders, it is possible to print NiTi alloy implants with desired properties. Implants printed with Ti-rich powders tend to exhibit SME property, while those printed with Ni-rich powders exhibit SE property at room temperature [260–262]. Although the Young's modulus of NiTi is higher than that of natural bone, it can be reduced to 11–20.5 GPa for porous NiTi implants using 3D printing techniques [263,264].

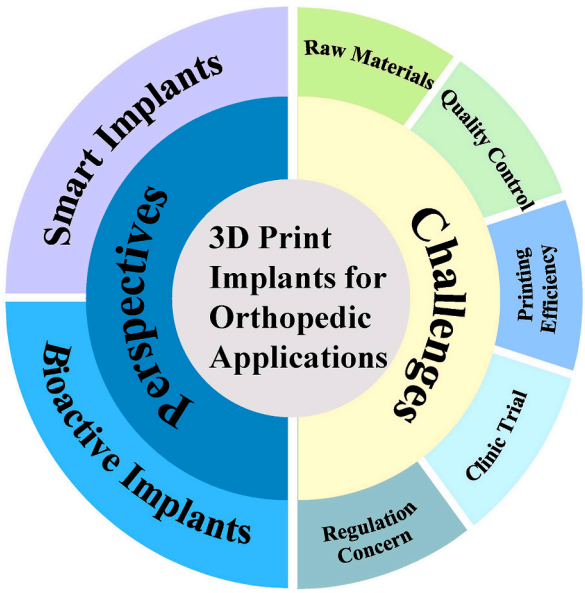

Fig. 7. Illustration of challenges and perspectives of the 3D print implants for orthopedic applications.

With biodegradability in body fluid environment, the biodegradable materials such as iron (Fe)-based alloys [86,265–268], magnesium (Mg)-based alloys [267,269–272] and zinc (Zn) based alloys [273–278] have attracted significant interest due to their superior biocompatibility and biodegradability in vivo. It is essential to continue exploring new materials for 3D printing in order to meet the evolving needs of medical applications and improve patient outcomes.

Fe-based alloys have sufficient strength for use in bone implants, but it is important to increase their in vivo corrosion rate to align with the healing process of bone tissues. Chou et al. [279] utilized the inkjet 3D printing technique to produce Fe–35Mn scaffolds. The porous scaffolds maintained similar mechanical property to natural bone, with an open porosity of 36.3%. They also demonstrated a desirable corrosion rate compared to pure iron, and the open pores allowed for cell infiltration. They suggested that Fe–Mn scaffolds were promising materials for craniofacial applications. Addition of Ca or Mg in the Fe–Mn scaffolds may further increase the corrosion rate without changing the biocompatibility [280]. Surface modification [281] and topological design [282] can also be conducted on 3D printed Fe scaffolds to improve osteogenesis property. Other printing materials with good biocompatibility can also be selected to fabricate iron-based implants [283].

Compared to Fe, Mg shows faster in vivo degradation rates and lower strength. However, the use of raw Mg powders for 3D printing is difficult and dangerous due to their high explosivity. To solve this issue, new methods such as mechanical crushing, atomization of motten metal, evaporation-condensation, and electrolysis have been employed for the fabrication of Mg powders. The powder size can also impact the quality of Mg-based depositions. A powder size less than 26 μm can lead to aggressive oxidation by raising the temperature of the melt pool, whereas large powder size (75–150 μm) may result in failing to form molten or sintered positions [284]. Small powder size increases the surface energy of Mg powder, which can cause powder splash during the printing process. Consequently, cracks, pockets, or cavities may appear on the printed implants [285]. Additionally, challenges such as highly affinity to oxygen and evaporation during heating hindered the manufacturing of Mg-based components using 3D printing techniques. However, recent advances, such as rapid, facile and extensible inkjet-based 3D printed methods have been successful in fabricating 3D printed Mg alloys [272,286–290]. By optimizing printing parameters (e.g., laser power, laser power density, laser scanning speed, layer thickness, and powder size), techniques such as SLM and wire arc additive manufacturing can also be applied to produce Mg-based 3D printed implants [285,291] This allows for Mg components to be fabricated with zero process contaminants. Moreover, the mechanical properties of Mg components can be tailored by the design of porous structures to match the mechanical properties of various types of bone.

Zn has also been regarded as a promising biodegradable metal material for orthopedic implants due to its proper degradation rate, which falls between that of Fe and Mg. However, with small difference between its low melting and boiling point, high vapor pressure, it is challenging and dangerous to fabricate porous Zn-based implants with 3D printing techniques. Nevertheless, a combination of 3D printing and traditional casting method has been successfully employed to produce Zn-based porous scaffold with varying porosity for bone tissue engineering. In this approach, 3D printing is utilized to produce a negative scaffold template, followed by lost salt suction casting to generate a pure Zn-based scaffold, without the need for advanced air circulation systems [292]. In recent developments, with optimal printing and gas flow parameters over the powder bed, laser powder bed fusion (LPBF) had been successfully applied to print Zn-based porous implants. Similar to Mg powders, the fabrication of Zn powders also has become one of the significant obstacles in LPBF for Zn implants [293]. Various fabrication methods have been proposed during the past years [294–296]. Fine Zn powders are more likely to be influenced by input laser energy. A high oxygen content can form on water-atomized Zn powders, making it difficult to print high-density implants [297]. Nonetheless, with appropriate printing parameters, high-density 3D printed Zn implants can achieve densities of about 99% [298]. In order to further improve the quality of Zn implants, Chen et al. have developed an optimized gas flow system that eliminates the negative effect of Zn metal evaporation on the processing of LPBF through numerical analysis [299] After optimizing the shielding flow and laser energy input, pure Zn implants with density over 99.90% have been produced. In addition to pure Zn implants, alloying elements or other reinforcement part can be added to improve the mechanical property of the Zn implants. For instance, the addition of rare earth cerium (Ce) to Zn using AM technique has significantly improved the ultimate tensile strength and creep resistance [300]. Yang et al. have selected the rare earth lanthanum (La) as a compatible interface layer between carbon nanofiber (CNF) and Zn matrix. This addition of La has significantly improved both the tensile strength and ductility of the CNF–La–Zn composites, and La has also enhanced the antitumor performance of the composites [301]. Notably, however, the Zn-based scaffold extracts have significantly reduced the viability of MC3T3-E1 cells [277], exhibiting much lower cytocompatibility than Ti6Al4V scaffolds [278]. As such, additional studies to better understand the biocompatibility of Zn-based porous implants are essential before clinical applications can occur.

4.1.2. Quality control

The exact geometrical structure of 3D printed orthopedic implants is typically determined by CAD models generated from medical images. Thus, high resolution medical images are of great importance to ensure the accuracy of 3D printing models. The segmentation, processing and printing of these models can directly affect the accuracy and quality of the resulting implants [302]. To achieve more precise models, thinner image cross-section slices are typically necessary. Additionally, the reconstruction kernel used must be carefully balanced for different applications since it can affect both the spatial resolution and image noise. Anisotropic mechanical behaviors are another characteristic of 3D printed components. This results in load-bearing capabilities that are different in the vertical and horizontal directions. To minimize this anisotropic behavior, post-processing procedures are applied, even with optimal structure design [303]. In certain situations, the printing precision may be insufficient for the printing of some fine structures. Waheed et al. [304] have suggested that printing resolutions higher than 10 μm are necessary for fabricating complex components with fine structures. While for the printing process, the printing directions and pathways must be designed carefully to minimize the divergence from design to execution.

4.1.3. Printing efficiency

To better understand the potential of 3D printing for future orthopedic implant applications, the printing time and cost of the implants should be further evaluated.

It is easy to regenerate 3D models with medical images, however, the segmentation or isolation of ROI is time-consuming and requires effort [305]. Although automated extraction algorithms have been developed to accelerate the segmentation and reconstruction speed for surgeons or engineers [306], manual extraction is still necessary for some complex cases with abnormal anatomy structures. Therefore, this limitation may restrict the use of 3D printing techniques in time sensitive and emergent cases requiring urgent intervention [307,308], and in cases where implant size is large and difficult to print. 3D processing software with a simplified and user-friendly interface should be developed. Customized implants can generally be printed in less than 24 h, with only rare cases taking longer. However, higher implant accuracy results in longer printing times. The balance between printing time and printing precision should be sought. Improving the hardware performance and developing new 3D printing process may shorten the preparation time for the implants.

For medical institutions, the costs for 3D printing includes hardware, software, printing raw materials, and other services. Despite the fact that the price of 3D printing is decreasing due to the fast development of new technology, it still requires a large initial investment. Consumer level 3D printers are now available at a low price, but these printers are less likely to fulfil the clinic requirements. To reduce costs, it has been suggested to use free or open-source software. Collaboration with other institutions may also help to share the costs.

4.1.4. Clinic trial

Up to now, plenty of clinic trails regarding 3D printed implants for different orthopedic applications have been reported [309–311]. The majority of the clinic outcomes showed superiority over conventional implants in terms of osteogenesis and complication rates. However, most of the reported clinic trails are case studies, and randomized and multi-center trials are lacking, which hinders the systematic comparison of the advantages and disadvantages between 3D-printed implants and traditional implants. In the future, more clinic trails and long-term follow up studies should be conducted [312].

4.1.5. Regulation concerns

As Class III medical devices, 3D printed implants must be approved by related regulatory authorities prior to commercialization. In the United States, the USA Food and Drug Administration (FDA) issued the first document entitled "Technical consideration for additive manufacture medical devices Guidance for industry and food and drug administration staff" for 3D printed medical devices. Currently, 3D printed medical devices should be reviewed and regulated under premarket notification [510(k)] and new drug application (NDA) pathways in USA [313,314]. In the early days, there were no such laws or regulations governing 3D-printed medical devices in China. However, with the fast-increasing number of reported clinical trials in China, it is of great importance to issue relevant regulations or acts to guide these clinic trials. Fortunately, the Chinese government and related regulatory authorities are now working together to address these issues and promote the use of 3D printed implants in clinical applications. In 2019, National Medical Products Administration (NMPA) issued the "Regulation on the Supervision and Administration of Custom-Made Medical Device", and in 2020, the Center for Medical Device Evaluation in the NMPA issued guidelines for the technical review of the registration of 3D printed artificial vertebral bodies and acetabular cups. These regulations and guidelines provide detailed procedures and requirements for researchers and medical device companies to improve their products. We believed that these regulations and guidelines will undoubtedly promote the development of 3D printed implants for orthopedic applications.

4.2. Future directions

With its great potential for printing implants with varying and complex structures, 3D printing is now regarded as an advanced and versatile manufacturing technique. Moving forward, despite the challenges we are facing currently, there are still improvements that can be made to further enhance the clinical usability of implants and the benefits they bring to patients and society.

In some instances, the clinic image dataset for 3D reconstruction or 3D printing may have a poor resolution, making it difficult to meet the basic requirements for further processing. Proper data augmentation algorithm can be applied to enhance the size and quality of the raw image datasets. Based on convolutional neural networks (CNNs) and generative adversarial networks (GANs), deep learning models have been applied [315]. Despite the fact that 3D printing is playing a vital role in personalized othopedic implant applications, optimizing printing parameters for 3D printing remains a challenge. In this regard, machine learning (ML) with artificial neural network (ANN) can be adopted to carry out intricate pattern identification and find the correlation between process parameters and the final characteristics of the printed component [316]. The combination of ANN models and particle swarm optimization algorithms has successfully been applied to minimize the surface roughness with optimized 3D printing process parameters [317]. Additionally, artificial intelligence (AI) algorithms and FEA are useful tools for simulating or predicting the mechanical behavior of the implants with designed structure [318,319].

4.2.1. Smart implants

The future 3D printed implants will not be limited to inanimate structures as previously printed. Smart materials, which can respond to environment stimuli such as heat and force over time have become hot topics in biomaterial scientific research. The combination of 3D printing techniques and smart materials may represent a new direction for 3D printing implants. Shape memory alloys (SMA) are the most common smart materials, although they can be difficult to fabricate using traditional machining methods.

SLM has been reported to be capable to producing complex Nickel–Titanium (Ni–Ti) SMA components [320,321] with favorable biocompatibility [322]. Electronic devices such as sensors can also be combined with implants to detect loading forces [323] and the physicochemical properties [324–326] of the surrounding body fluids in-suit. Such combinations can help improve our understanding of the in vivo performance of implants.

4.2.2. Bioactive implants

Improving the biological functions of 3D printed implants is an efficiency way to shorten the healing time and reduce complication rate [115,327]. Proper surface treatment may enhance the adhesion and absorbance of the cells and proteins to form a better implants-tissues interface. Addition of growth factors [328], functional molecules [329], peptides or proteins [330–332] in the coatings can increase the osteogenesis property, promote vessel formation within the implants, and inhibit bacterial proliferation [333, 334]. Although 3D printed polymers or hydrogels with cells or growth factors have improved the biological activity of the implants, their inherent insufficient mechanical property have limited the usage in load bearing applications. Infiltration of these material-cell composites into the porous 3D printed implants may further improve the in vitro and in vivo performances [335,336]. The pores within the implants also provide an ideal vehicle for drug delivery [337]. By loading chemotherapy or antimicrobial drugs, 3D printed implants may be effective in treating tumor recurrences [338] or infections [339].

5. Conclusion

Nowadays, 3D printing is recognized as a revolutionary key technology in personalized medicine due to its ability to provide customized orthopedic implants. Since the invention of 3D printing technique, it has had a profound impact on medical implants. By combining medical images with 3D printing techniques, the usage of 3D printed implants in orthopedic applications has been broadened. With the efforts of surgeons and engineers, several clinic usages of 3D printed implants have been reported in the last few decades. These early attempts have clearly proven 3D printing to be an effective choice for orthopedic applications. And it is believed that 3D printing has the potential to revolutionize future orthopedic practices. Although, challenges and barriers exist in the current state of the technology, the future of 3D printing in orthopedic applications is still relatively bright and 3D printing is a promising technique that can help overcome some difficult clinical issues. As more and more professional researchers are recruited into the 3D printing field, together with the continuous advances in hardware, software, imaging and regulation, it is likely that 3D printed implants will rapidly improve and eventually become widely commercially available on the market in the coming years.

Author contribution statement

All authors listed have significantly contributed to the development and the writing of this article.

Data availability statement

No data was used for the research described in the article.

Declaration of competing interest

The authors declare that they have no known competing financial interests or personal relationships that could have appeared to influence the work reported in this paper.

Acknowledgements

This work was supported by the National Natural Science Foundation of China (Grant No. 81902193 and 82172450), Beijing Municipal Natural Science Foundation (7202167); CAMS Innovation Fund for Medical Sciences(CIFMS, No. 2020-I2M-C&T-B-025)

References

[1] Y. Huang, M.C. Leu, J. Mazumder, et al., Additive manufacturing: current state, future potential, gaps and needs, and recommendations, J. Manuf. Sci. E.-T. Asme 137 (1) (2015), 014001.
[2] ASTM, *ASTM International Committee*, F42 on additive manufacturing technologies, in: ASTM F2792-10 Standard Terminology for Additive Manufacturing Technologies, ASTM, West Conshohocken, PA, 2009.
[3] S.V. Murphy, A. Atala, 3D bioprinting of tissues and organs, Nat. Biotechnol. 32 (8) (2014) 773–785.
[4] A. Vafadar, F. Guzzomi, A. Rassau, et al., Advances in metal additive manufacturing: a review of common processes, industrial applications, and current challenges, Applied Sciences-Basel 11 (3) (2021).
[5] H. Wu, W.P. Fahy, S. Kim, et al., Recent developments in polymers/polymer nanocomposites for additive manufacturing, Prog. Mater. Sci. 111 (2020) 10638.
[6] N. van de Werken, H. Tekinalp, P. Khanbolouki, et al., Additively manufactured carbon fiber-reinforced composites: state of the art and perspective, Addit. Manuf. 31 (2020), 100962.
[7] Z.Q. Wan, P. Zhang, Y.S. Liu, et al., Four-dimensional bioprinting: current developments and applications in bone tissue engineering, Acta Biomater. 101 (2020) 26–42.
[8] R. Langer, J.P. Vacanti, Tissue engineering, Science 260 (5110) (1993) 920–926.
[9] F. Rengier, A. Mehndiratta, H. von Tengg-Kobligk, et al., 3D printing based on imaging data: review of medical applications, Int. J. Comput. Assist. Radiol. Surg. 5 (4) (2010) 335–341.

[10] D.H. Frakes, M.J.T. Smith, J. Parks, et al., New techniques for the reconstruction of complex vascular anatomies from MRI images, J. Cardiovasc. Magn. Reson. 7 (2) (2005) 425–432.
[11] G. Castrisos, I. Gonzalez Matheus, D. Sparks, et al., Regenerative matching axial vascularisation of absorbable 3D-printed scaffold for large bone defects: a first in human series, J. Plast. Reconstr. Aesthetic Surg. 75 (7) (2022) 2108–2118.
[12] G. Valente, M.G. Benedetti, M. Paolis, et al., Long-term functional recovery in patients with custom-made 3D-printed anatomical pelvic prostheses following bone tumor excision, Gait Posture 97 (2022) 73–79.
[13] J. Zhang, R. Zhang, G. Ren, et al., A method for using solid modeling CAD software to create an implant library for the fabrication of a custom abutment, J. Prosthet. Dent 117 (2) (2017) 209–213.
[14] J. Kang, E. Dong, X. Li, et al., Topological design and biomechanical evaluation for 3D printed multi-segment artificial vertebral implants, Mater Sci Eng C Mater Biol Appl 127 (2021) 112250.
[15] M. Cronskär, L.-E. Rännar, M. Bäckström, Implementation of digital design and solid free-form fabrication for customization of implants in trauma orthopaedics, J. Med. Biol. Eng. 32 (2012) 91–96.
[16] J. Ding, Q. Zou, S. Qu, et al., STL-free design and manufacturing paradigm for high-precision powder bed fusion, CIRP Annals 70 (1) (2021) 167–170.
[17] J.S. Akmal, M. Salmi, B. Hemming, et al., Cumulative inaccuracies in implementation of additive manufacturing through medical imaging, 3D thresholding, and 3D modeling: a case study for an end-use implant, Appl. Sci. 10 (8) (2020) 2968.
[18] Y. Liu, S.L. Sing, R.X.E. Lim, et al., Preliminary investigation on the geometric accuracy of 3D printed dental implant using a monkey maxilla incisor model, Int J Bioprint 8 (1) (2022) 2476.
[19] C. Kopsacheilis, P. Charalampous, I. Kostavelis, et al., In situ visual quality control in 3D printing, VISIGRAPP (2020).
[20] M. Fogarasi, J.C. Coburn, B. Ripley, Algorithms used in medical image segmentation for 3D printing and how to understand and quantify their performance, 3D Print, Med 8 (1) (2022) 18.
[21] S. Kachhara, D. Nallaswamy, D.M. Ganapathy, et al., Comparison of the CBCT, CT, 3D printing, and CAD-CAM Milling options for the most accurate root form duplication required for the root analogue implant (RAI) protocol, J. Indian Acad. Oral Med. Radiol. 33 (2021) 141–145.
[22] S. Weidert, S. Andress, E. Suero, et al., 3D-Druck in der unfallchirurgischen Fort- und Weiterbildung, Unfallchirurg 122 (6) (2019) 444–451.
[23] M.R. Urist, Bone: formation by autoinduction, Science 150 (3698) (1965) 893–899.
[24] V. Karageorgiou, D. Kaplan, Porosity of 3D biomaterial scaffolds and osteogenesis, Biomaterials 26 (27) (2005) 5474–5491.
[25] S.J. Hollister, Scaffold design and manufacturing: from concept to clinic, Adv. Mater. 21 (32–33) (2009) 3330–3342.
[26] X.J. Wang, S.Q. Xu, S.W. Zhou, et al., Topological design and additive manufacturing of porous metals for bone scaffolds and orthopaedic implants: a review, Biomaterials 83 (2016), 127-141.
[27] S.I. Roohani-Esfahani, P. Newman, H. Zreiqat, Design and fabrication of 3D printed scaffolds with a mechanical strength comparable to cortical bone to repair large bone defects, Sci. Rep. 6 (2016), 19468.
[28] L.G. Sicchieri, G.E. Crippa, P.T. de Oliveira, et al., Pore size regulates cell and tissue interactions with PLGA-CaP scaffolds used for bone engineering, J. Tissue Eng. Regen. Med. 6 (2) (2012) 155–162.
[29] F.S.L. Bobbert, A.A. Zadpoor, Effects of bone substitute architecture and surface properties on cell response, angiogenesis, and structure of new bone, J. Mater. Chem. B 5 (31) (2017) 6175–6192.
[30] S.J. Hollister, Porous scaffold design for tissue engineering, Nat. Mater. 4 (7) (2005) 518–524.
[31] A.I. Itälä, H.O. Ylänen, C. Ekholm, et al., Pore diameter of more than 100 μm is not requisite for bone ingrowth in rabbits, J. Biomed. Mater. Res. 58 (6) (2001) 679–683.
[32] Y. Kuboki, Q.M. Jin, H. Takita, Geometry of carriers controlling phenotypic expression in BMP-induced osteogenesis and chondrogenesis, J. Bone Joint Surg. Am. 83a (2001). S105-S115.
[33] N. Taniguchi, S. Fujibayashi, M. Takemoto, et al., Effect of pore size on bone ingrowth into porous titanium implants fabricated by additive manufacturing: an in vivo experiment, Mat. Sci. Eng. C-Mater. 59 (2016) 690–701.
[34] Q.C. Ran, W.H. Yang, Y. Hu, et al., Osteogenesis of 3D printed porous Ti6Al4V implants with different pore sizes, J. Mech. Behav. Biomed. Mater. 84 (2018) 1–11.
[35] D.W. Hutmacher, Scaffolds in tissue engineering bone and cartilage, Biomaterials 21 (24) (2000) 2529–2543.
[36] H. Seyednejad, D. Gawlitta, R.V. Kuiper, et al., In vivo biocompatibility and biodegradation of 3D-printed porous scaffolds based on a hydroxyl-functionalized poly(epsilon-caprolactone), Biomaterials 33 (17) (2012) 4309–4318.
[37] Q.Q. Yao, J.G.L. Cosme, T. Xu, et al., Three dimensional electrospun PCL/PLA blend nanofibrous scaffolds with significantly improved stem cells osteogenic differentiation and cranial bone formation, Biomaterials 115 (2017), 115-127.
[38] C.H. Gao, C.Y. Wang, H. Jin, et al., Additive manufacturing technique-designed metallic porous implants for clinical application in orthopedics, Rsc Adv 8 (44) (2018) 25210–25227.
[39] J. Van der Stok, O.P. Van der Jagt, S.A. Yavari, et al., Selective laser melting-produced porous titanium scaffolds regenerate bone in critical size cortical bone defects, J. Orthop. Res. 31 (5) (2013) 792–799.
[40] A. Bandyopadhyay, F. Espana, V.K. Balla, et al., Influence of porosity on mechanical properties and in vivo response of Ti6Al4V implants, Acta Biomater. 6 (4) (2010) 1640–1648.
[41] D.A. Shimko, V.F. Shimko, E.A. Sander, et al., Effect of porosity on the fluid flow characteristics and mechanical properties of tantalum scaffolds, J. Biomed. Mater. Res. B 73b (2) (2005) 315–324.
[42] R.A. Perez, G. Mestres, Role of pore size and morphology in musculo-skeletal tissue regeneration, Mat. Sci. Eng. C-Mater. 61 (2016) 922–939.
[43] J.P. Li, P. Habibovic, M. van den Doel, et al., Bone ingrowth in porous titanium implants produced by 3D fiber deposition, Biomaterials 28 (18) (2007) 2810–2820.
[44] C.N. Kelly, A.T. Miller, S.J. Hollister, et al., Design and structure-function characterization of 3D printed synthetic porous biomaterials for tissue engineering, Adv. Healthc. Mater. 7 (7) (2018), e1701095.
[45] J.M. Kemppainen, S.J. Hollister, Differential effects of designed scaffold permeability on chondrogenesis by chondrocytes and bone marrow stromal cells, Biomaterials 31 (2) (2010) 279–287.
[46] A.G. Mitsak, J.M. Kemppainen, M.T. Harris, et al., Effect of polycaprolactone scaffold permeability on bone regeneration in vivo, Tissue Eng. 17 (13–14) (2011) 1831–1839.
[47] E. Askari, I.F. Cengiz, J.L. Alves, et al., Micro-CT based finite element modelling and experimental characterization of the compressive mechanical properties of 3-D zirconia scaffolds for bone tissue engineering, J. Mech. Behav. Biomed. Mater. 102 (2020), 103516.
[48] R. Noroozi, F. Tatar, A. Zolfagharian, et al., Additively manufactured multi-morphology bone-like porous scaffolds: experiments and micro-computed tomography-based finite element modeling approaches, Int J Bioprint 8 (3) (2022) 2556.
[49] R.B. Osman, A.J. van der Veen, D. Huiberts, et al., 3D-printing zirconia implants; a dream or a reality? An in-vitro study evaluating the dimensional accuracy, surface topography and mechanical properties of printed zirconia implant and discs, J. Mech. Behav. Biomed. Mater. 75 (2017) 521–528.
[50] N. Otawa, T. Sumida, H. Kitagaki, et al., Custom-made titanium devices as membranes for bone augmentation in implant treatment: modeling accuracy of titanium products constructed with selective laser melting, J. Cranio-Maxillo-Fac. Surg. 43 (7) (2015) 1289–1295.
[51] J. Ni, H. Ling, S. Zhang, et al., Three-dimensional printing of metals for biomedical applications, Mater Today Bio 3 (2019), 100024.
[52] S. Zhou, W. Li, G. Sun, et al., A level-set procedure for the design of electromagnetic metamaterials, Opt Express 18 (7) (2010) 6693–6702.
[53] S.J. Hollister, R.D. Maddox, J.M. Taboas, Optimal design and fabrication of scaffolds to mimic tissue properties and satisfy biological constraints, Biomaterials 23 (20) (2002) 4095–4103.
[54] C.Y. Lin, N. Kikuchi, S.J. Hollister, A novel method for biomaterial scaffold internal architecture design to match bone elastic properties with desired porosity, J. Biomech. 37 (5) (2004) 623–636.

[55] Y.H. Chen, J.E. Frith, A. Dehghan-Manshadi, et al., Mechanical properties and biocompatibility of porous titanium scaffolds for bone tissue engineering, J. Mech. Behav. Biomed. Mater. 75 (2017) 169–174.
[56] X.Y. Zhang, G. Fang, J. Zhou, Additively manufactured scaffolds for bone tissue engineering and the prediction of their mechanical behavior: a review, Materials 10 (1) (2017) 2050.
[57] S. Arabnejad, R.B. Johnston, J.A. Pura, et al., High-strength porous biomaterials for bone replacement: a strategy to assess the interplay between cell morphology, mechanical properties, bone ingrowth and manufacturing constraints, Acta Biomater. 30 (2016) 345–356.
[58] S. Ponader, C. von Wilmowsky, M. Widenmayer, et al., In vivo performance of selective electron beam-melted Ti-6Al-4V structures, J. Biomed. Mater. Res. 92a (1) (2010) 56–62.
[59] S. Van Bael, Y.C. Chai, S. Truscello, et al., The effect of pore geometry on the in vitro biological behavior of human periosteum-derived cells seeded on selective laser-melted Ti6Al4V bone scaffolds, Acta Biomater. 8 (7) (2012) 2824–2834.
[60] H. Wang, K.X. Su, L.Z. Su, et al., The effect of 3D-printed Ti6Al4V scaffolds with various macropore structures on osteointegration and osteogenesis: a biomechanical evaluation, J. Mech. Behav. Biomed. Mater. 88 (2018) 488–496.
[61] J. Wieding, A. Wolf, R. Bader, Numerical optimization of open-porous bone scaffold structures to match the elastic properties of human cortical bone, J. Mech. Behav. Biomed. Mater. 37 (2014) 56–68.
[62] J. An, J.E.M. Teoh, R. Suntornnond, et al., Design and 3D printing of scaffolds and tissues, Engineering 1 (2) (2015) 261–268.
[63] F.S.L. Bobbert, K. Lietaert, A.A. Eftekhari, et al., Additively manufactured metallic porous biomaterials based on minimal surfaces: a unique combination of topological, mechanical, and mass transport properties, Acta Biomater. 53 (2017) 572–584.
[64] N. Sudarmadji, J.Y. Tan, K.F. Leong, et al., Investigation of the mechanical properties and porosity relationships in selective laser-sintered polyhedral for functionally graded scaffolds, Acta Biomater. 7 (2) (2011) 530–537.
[65] S. Wang, L.L. Liu, K. Li, et al., Pore functionally graded Ti6Al4V scaffolds for bone tissue engineering application, Mater. Des. 168 (2019), 107643.
[66] X.Y. Zhang, G. Fang, L.L. Xing, et al., Effect of porosity variation strategy on the performance of functionally graded Ti-6Al-4V scaffolds for bone tissue engineering, Mater. Des. 157 (2018) 523–538.
[67] H. Kang, Y.Z. Zeng, S. Varghese, Functionally graded multilayer scaffolds for in vivo osteochondral tissue engineering, Acta Biomater. 78 (2018) 365–377.
[68] A. Boccaccio, A.E. Uva, M. Fiorentino, et al., Geometry design optimization of functionally graded scaffolds for bone tissue engineering: a mechanobiological approach, PLoS One 11 (1) (2016), e0146935.
[69] S. Ozkan, D.M. Kalyon, X.J. Yu, Functionally graded beta-TCP/PCL nanocomposite scaffolds: in vitro evaluation with human fetal osteoblast cells for bone tissue engineering, J. Biomed. Mater. Res. 92a (3) (2010) 1007–1018.
[70] K.F. Leong, C.K. Chua, N. Sudarmadji, et al., Engineering functionally graded tissue engineering scaffolds, J. Mech. Behav. Biomed. Mater. 1 (2) (2008) 140–152.
[71] P. Heinl, L. Muller, C. Korner, et al., Cellular Ti-6Al-4V structures with interconnected macro porosity for bone implants fabricated by selective electron beam melting, Acta Biomater. 4 (5) (2008) 1536–1544.
[72] P. Heinl, A. Rottmair, C. Korner, et al., Cellular titanium by selective electron beam melting, Adv. Eng. Mater. 9 (5) (2007) 360–364.
[73] M.A. Surmeneva, R. Surmenev, E.A. Chudinova, et al., Fabrication of multiple-layered gradient cellular metal scaffold via electron beam melting for segmental bone reconstruction, Mater. Des. 133 (2017) 195–204.
[74] C.J. Han, Y. Li, Q. Wang, et al., Continuous functionally graded porous titanium scaffolds manufactured by selective laser melting for bone implants, J. Mech. Behav. Biomed. Mater. 80 (2018) 119–127.
[75] K.C. Nune, A. Kumar, R.D.K. Misra, et al., Functional response of osteoblasts in functionally gradient titanium alloy mesh arrays processed by 3D additive manufacturing, Colloids Surf., B 150 (2017) 78–88.
[76] K. Song, Z. Wang, J. Lan, et al., Porous structure design and mechanical behavior analysis based on TPMS for customized root analogue implant, J. Mech. Behav. Biomed. Mater. 115 (2021), 104222.
[77] Z. Li, Z. Chen, X. Chen, et al., Mechanical properties of triply periodic minimal surface (TPMS) scaffolds: considering the influence of spatial angle and surface curvature, Biomech. Model. Mechanobiol. (2022).
[78] B. Liao, R.F. Xia, W. Li, et al., 3D-Printed Ti6Al4V scaffolds with graded triply periodic minimal surface structure for bone tissue engineering, J. Mater. Eng. Perform. 30 (7) (2021) 4993–5004.
[79] M. Speirs, B. Van Hooreweder, J. Van Humbeeck, et al., Fatigue behaviour of NiTi shape memory alloy scaffolds produced by SLM, a unit cell design comparison, J. Mech. Behav. Biomed. Mater. 70 (2017) 53–59.
[80] J. Zhang, X. Chen, Y. Sun, et al., Design of a biomimetic graded TPMS scaffold with quantitatively adjustable pore size, Mater. Des. 218 (2022), 110665.
[81] S.V. Balabanov, A.I. Makogon, M.M. Sychov, et al., Mechanical properties of 3D printed cellular structures with topology of triply periodic minimal surfaces, Mater. Today: Proc. 30 (2020) 439–442.
[82] N.V. Viet, W. Waheed, A. Alazzam, et al., Effective compressive behavior of functionally graded TPMS titanium implants with ingrown cortical or trabecular bone, Compos. Struct. 303 (2023), 116288.
[83] J.P. Shi, J.Q. Yang, Z.A. Li, et al., Design and fabrication of graduated porous Ti-based alloy implants for biomedical applications, J. Alloys Compd. 728 (2017) 1043–1048.
[84] A.A. Zadpoor, J. Malda, Additive manufacturing of biomaterials, tissues, and organs, Ann. Biomed. Eng. 45 (1) (2017).
[85] Y.C. Wu, C.N. Kuo, M.Y. Shie, et al., Structural design and mechanical response of gradient porous Ti-6Al-4V fabricated by electron beam additive manufacturing, Mater. Des. 158 (2018) 256–265.
[86] Y. Li, H. Jahr, P. Pavanram, et al., Additively manufactured functionally graded biodegradable porous iron, Acta Biomater. 96 (2019) 646–661.
[87] T.D. Ngo, A. Kashani, G. Imbalzano, et al., Additive manufacturing (3D printing): a review of materials, methods, applications and challenges, Compos. B Eng. 143 (2018) 172–196.
[88] C.Y. Yap, C.K. Chua, Z.L. Dong, et al., Review of selective laser melting: materials and applications, Appl. Phys. Rev. 2 (4) (2015), 041101.
[89] J.J. Lewandowski, M. Seifi, Metal additive manufacturing: a review of mechanical properties, Annu. Rev. Mater. Res. 46 (2016) 151–186.
[90] W.E. Frazier, Metal additive manufacturing: a review, J. Mater. Eng. Perform. 23 (6) (2014) 1917–1928.
[91] E. Wycisk, A. Solbach, S. Siddique, et al., Effects of defects in laser additive manufactured Ti-6Al-4V on fatigue properties, Phys. Procedia 56 (2014) 371–378.
[92] T. DebRoy, H.L. Wei, J.S. Zuback, et al., Additive manufacturing of metallic components - process, structure and properties, Prog. Mater. Sci. 92 (2018) 112–224.
[93] M. Wang, Y. Wu, S. Lu, et al., Fabrication and characterization of selective laser melting printed Ti–6Al–4V alloys subjected to heat treatment for customized implants design, Prog. Nat. Sci.: Mater. Int. 26 (6) (2016) 671–677.
[94] E. Wycisk, S. Siddique, D. Herzog, et al., Fatigue Performance of laser additive Manufactured Ti-6al-4V in Very high cycle Fatigue regime up to 10(9) cycles, Front. Mater. 2 (2015) 72.
[95] A. Mohammadhosseini, D. Fraser, S.H. Masood, et al., Compressive properties of Ti-6Al-4V built by electron beam melting, Adv. Mater. Res. 811 (2013) 108–112.
[96] G. Kasperovich, J. Hausmann, Improvement of fatigue resistance and ductility of TiAl6V4 processed by selective laser melting, J. Mater. Process. Technol. 220 (2015) 202–214.
[97] P. Jamshidi, M. Aristizabal, W.H. Kong, et al., Selective laser melting of Ti-6Al-4V: the impact of post-processing on the tensile, fatigue and biological properties for medical implant applications, Materials 13 (12) (2020) 2813.
[98] M.W. Wu, J.K. Chen, B.H. Lin, et al., Improved fatigue endurance ratio of additive manufactured Ti-6Al-4V lattice by hot isostatic pressing, Mater. Des. 134 (2017) 163–170.
[99] A. Hemmasian Ettefagh, C. Zeng, S. Guo, et al., Corrosion behavior of additively manufactured Ti-6Al-4V parts and the effect of post annealing, Addit. Manuf. 28 (2019) 252–258.

[100] S.L. Sing, J. An, W.Y. Yeong, et al., Laser and electron-beam powder-bed additive manufacturing of metallic implants: a review on processes, materials and designs, J. Orthop. Res. 34 (3) (2016) 369–385.
[101] S.A. Yavari, S.M. Ahmadi, J. van der Stok, et al., Effects of bio-functionalizing surface treatments on the mechanical behavior of open porous titanium biomaterials, J. Mech. Behav. Biomed. Mater. 36 (2014) 109–119.
[102] D. Tang, R.S. Tare, L.Y. Yang, et al., Biofabrication of bone tissue: approaches, challenges and translation for bone regeneration, Biomaterials 83 (2016), 363-382.
[103] K. Anselme, M. Bigerelle, B. Noel, et al., Qualitative and quantitative study of human osteoblast adhesion on materials with various surface roughnesses, J. Biomed. Mater. Res. 49 (2) (2000) 155–166.
[104] M. Lai, C.D. Hermann, A. Cheng, et al., Role of alpha 2 beta 1 integrins in mediating cell shape on microtextured titanium surfaces, J. Biomed. Mater. Res. 103 (2) (2015) 564–573.
[105] Z.H. Li, C. Liu, B.F. Wang, et al., Heat treatment effect on the mechanical properties, roughness and bone ingrowth capacity of 3D printing porous titanium alloy, Rsc Adv 8 (22) (2018) 12471–12483.
[106] S. Ponader, E. Vairaktaris, P. Heinl, et al., Effects of topographical surface modifications of electron beam melted Ti-6Al-4V titanium on human fetal osteoblasts, J. Biomed. Mater. Res. 84a (4) (2008) 1111–1119.
[107] R. Olivares-Navarrete, S.L. Hyzy, J.H. Park, et al., Mediation of osteogenic differentiation of human mesenchymal stem cells on titanium surfaces by a Wnt-integrin feedback loop, Biomaterials 32 (27) (2011) 6399–6411.
[108] R. Olivares-Navarrete, P. Raz, G. Zhao, et al., Integrin α2β1 plays a critical role in osteoblast response to micron-scale surface structure and surface energy of titanium substrates, Proc. Natl. Acad. Sci. U.S.A. 105 (41) (2008) 15767–15772.
[109] E. Garcia-Gareta, M.J. Coathup, G.W. Blunn, Osteoinduction of bone grafting materials for bone repair and regeneration, Bone 81 (2015) 112–121.
[110] P. Habibovic, K. de Groot, Osteoinductive biomaterials - properties and relevance in bone repair, J. Tissue Eng. Regen. Med. 1 (1) (2007) 25–32.
[111] P. Xiu, Z.J. Jia, J. Lv, et al., Tailored surface treatment of 3D printed porous Ti6Al4V by microarc oxidation for enhanced osseointegration via optimized bone in-growth patterns and interlocked bone/implant interface, ACS Appl. Mater. Interfaces 8 (28) (2016) 17964–17975.
[112] M.T. Arafat, C.X.F. Lam, A.K. Ekaputra, et al., Biomimetic composite coating on rapid prototyped scaffolds for bone tissue engineering, Acta Biomater. 7 (2) (2011) 809–820.
[113] Z.F. Huang, Z.H. Wu, B.P. Ma, et al., Enhanced in vitro biocompatibility and osteogenesis of titanium substrates immobilized with dopamine-assisted superparamagnetic Fe3O4 nanoparticles for hBMSCs, R. Soc. Open Sci. 5 (8) (2018), 172033.
[114] Y. He, L.J. Yu, J.Y. Liu, et al., Enhanced osteogenic differentiation of human bone-derived mesenchymal stem cells in 3-dimensional printed porous titanium scaffolds by static magnetic field through up-regulating Smad4, Faseb. J. 33 (5) (2019) 6069–6081.
[115] S. Bose, S.F. Robertson, A. Bandyopadhyay, Surface modification of biomaterials and biomedical devices using additive manufacturing, Acta Biomater. 66 (2018) 6–22.
[116] P. Rider, Z.P. Kacarevic, S. Alkildani, et al., Additive manufacturing for guided bone regeneration: a perspective for alveolar ridge augmentation, Int. J. Mol. Sci. 19 (11) (2018) 3308.
[117] M.P. Chae, W.M. Rozen, P.G. McMenamin, et al., Emerging applications of bedside 3D printing in plastic surgery, Front. Surg. 2 (25) (2015) 2025.
[118] S.C. Fuller, M.G. Moore, Additive manufacturing technology in reconstructive surgery, Curr. Opin. Otolaryngol. Head Neck Surg. 24 (5) (2016) 420–425.
[119] N. Tellisi, N.A. Ashammakhi, F. Billi, et al., Three dimensional printed bone implants in the clinic, J. Craniofac. Surg. 29 (8) (2018) 2363–2367.
[120] P. Tack, J. Victor, P. Gemmel, et al., 3D-printing techniques in a medical setting: a systematic literature review, Biomed. Eng. Online 15 (2016) 115.
[121] H. Xu, D. Han, J.S. Dong, et al., Rapid prototyped PGA/PLA scaffolds in the reconstruction of mandibular condyle bone defects, Int. J. Med. Robot. 6 (1) (2010) 66–72.
[122] S. Haimi, N. Suuriniemi, A.M. Haaparanta, et al., Growth and osteogenic differentiation of adipose stem cells on PLA/bioactive glass and PLA/beta-TCP scaffolds, Tissue Eng. 15 (7) (2009) 1473–1480.
[123] H. Saijo, K. Igawa, Y. Kanno, et al., Maxillofacial reconstruction using custom-made artificial bones fabricated by inkjet printing technology, J. Artif. Organs 12 (3) (2009) 200–205.
[124] U. Klammert, U. Gbureck, E. Vorndran, et al., 3D powder printed calcium phosphate implants for reconstruction of cranial and maxillofacial defects, J. Cranio-Maxillo-Fac. Surg. 38 (8) (2010) 565–570.
[125] L. Meseguer-Olmo, V. Vicente-Ortega, M. Alcaraz-Banos, et al., In-vivo behavior of Si-hydroxyapatite/polycaprolactone/DMB scaffolds fabricated by 3D printing, J. Biomed. Mater. Res. 101 (7) (2013) 2038–2048.
[126] E. Farre-Guasch, J. Wolff, M.N. Helder, et al., Application of additive manufacturing in oral and maxillofacial surgery, J. Oral Maxillofac. Surg. 73 (12) (2015) 2408–2418.
[127] N. Fernandes, J. van den Heever, C. Hoogendijk, et al., Reconstruction of an extensive midfacial defect using additive manufacturing techniques, J. Prosthodont. 25 (7) (2016) 589–594.
[128] M.E. Roos, J. Claassen, G. Booysen, et al., 3D printed titanium prosthesis reconstruction following subtotal maxillectomy for myoepithelial carcinoma - a case report, J Stomatol Oral Maxillofac Surg 121 (2) (2020) 175–178.
[129] S.R. Liu, X.F. Song, Z.K. Li, et al., Postoperative improvement of diplopia and extraocular muscle movement in patients with reconstructive surgeries for orbital floor fractures, J. Craniofac. Surg. 27 (8) (2016) 2043–2049.
[130] M.A. Gavin Clavero, M.V. Simon Sanz, A.M. Til, et al., Factors influencing postsurgical diplopia in orbital floor fractures and prevalence of other complications in a series of cases, J. Oral Maxillofac. Surg. 76 (8) (2018) 1725–1733.
[131] A. Gonzalez Alvarez, S. Ananth, L. Dovgalski, et al., Custom three-dimensional printed orbital plate composed of two joined parts with variable thickness for a large orbital floor reconstruction after post-traumatic zygomatic fixation, Br. J. Oral Maxillofac. Surg. 58 (10) (2020) e341–e342.
[132] U.L. Lee, J.S. Kwon, S.H. Woo, et al., Simultaneous bimaxillary surgery and mandibular reconstruction with a 3-dimensional printed titanium implant fabricated by electron beam melting: a preliminary mechanical testing of the printed mandible, J. Oral Maxillofac. Surg. 74 (7) (2016) 1501.
[133] M. Salmi, J. Tuomi, K.S. Paloheimo, et al., Patient-specific reconstruction with 3D modeling and DMLS additive manufacturing, Rapid Prototyp. J. 18 (3) (2012) 209–214.
[134] K. Dowgierd, R. Pokrowiecki, M. Borowiec, et al., A protocol for the use of a combined microvascular free flap with custom-made 3D-printed total temporomandibular joint (TMJ) prosthesis for mandible reconstruction in children, Appl. Sci. 11 (5) (2021) 2176.
[135] M.Y. Mommaerts, Patient- and clinician-reported outcomes of lower jaw contouring using patient-specific 3D-printed titanium implants, Int. J. Oral Maxillofac. Surg. 50 (3) (2021) 373–377.
[136] G.S. Wang, J.H. Li, A. Khadka, et al., CAD/CAM and rapid prototyped titanium for reconstruction of ramus defect and condylar fracture caused by mandibular reduction, Oral Surg. Oral Med. Oral Pathol. Oral Radiol. 113 (3) (2012) 356–361.
[137] O.C. Thiele, I.M. Nolte, R.A. Mischkowski, et al., Craniomaxillofacial patient-specific CAD/CAM implants based on cone-beam tomography data - a feasibility study, J. Cranio-Maxillo-Fac. Surg. 46 (9) (2018) 1461–1464.
[138] S.K. Malyala, Y.R. Kumar, A.M. Alwala, A 3D-printed osseointegrated combined jaw and dental implant prosthesis - a case study, Rapid Prototyp. J. 23 (6) (2017) 1164–1169.
[139] J. Ma, L. Ma, Z. Wang, et al., The use of 3D-printed titanium mesh tray in treating complex comminuted mandibular fractures, Medicine (Baltim.) 96 (27) (2017) e7250.
[140] Q. Qassemyar, N. Assouly, S. Temam, et al., Use of a three-dimensional custom-made porous titanium prosthesis for mandibular body reconstruction, Int. J. Oral Maxillofac. Surg. 46 (10) (2017) 1248–1251.
[141] J. Zheng, X. Chen, W. Jiang, et al., An innovative total temporomandibular joint prosthesis with customized design and 3D printing additive fabrication: a prospective clinical study, J. Transl. Med. 17 (1) (2019) 4.

[142] A. Gonzalez Alvarez, S. Ananth, L. Dovgalski, et al., Custom three-dimensional printed orbital plate composed of two joined parts with variable thickness for a large orbital floor reconstruction after post-traumatic zygomatic fixation, Br. J. Oral Maxillofac. Surg. 58 (10) (2020) e341–e342.
[143] X. Chen, Y. Mao, J. Zheng, et al., Clinical and radiological outcomes of Chinese customized three-dimensionally printed total temporomandibular joint prostheses: a prospective case series study, J. Plast. Reconstr. Aesthetic Surg. 74 (7) (2021) 1582–1593.
[144] K. Darwich, M.B. Ismail, M.Y.A.-S. Al-Mozaiek, et al., Reconstruction of mandible using a computer-designed 3D-printed patient-specific titanium implant: a case report, Oral Maxillofac. Surg. 25 (1) (2021) 103–111.
[145] P.A. Dearnley, A review of metallic, ceramic and surface-treated metals used for bearing surfaces in human joint replacements, Proc. Inst. Mech. Eng. H 213 (H2) (1999) 107–135.
[146] Z.H. Li, C.Y. Wang, C. Li, et al., What we have achieved in the design of 3D printed metal implants for application in orthopedics? Personal experience and review, Rapid Prototyp. J. 24 (8) (2018) 1365–1379.
[147] M. Godec, A. Kocijan, D. Dolinar, et al., An investigation of the aseptic loosening of an AISI 316L stainless steel hip prosthesis, Biomed. Mater. 5 (4) (2010), 045012.
[148] T. Lugli, Artificial shoulder joint by P??an (1893): the facts of an exceptional intervention and the prosthetic method, Clin. Orthop. 133 (133) (1978) 215–218.
[149] V.T. Deore, E. Griffiths, P. Monga, Shoulder arthroplasty-Past, present and future, J. Arthrosc. Joint Surg. 5 (5) (2018) 3–8.
[150] G. Beltrami, G. Ristori, G. Scoccianti, et al., Latissimus dorsi rotational flap combined with a custom-made scapular prosthesis after oncological surgical resection: a report of two patients, BMC Cancer 18 (2018) 1003.
[151] Q.A. Yang, J.M. Li, Z.P. Yang, et al., Limb sparing surgery for bone tumours of the shoulder girdle: the oncological and functional results, Int. Orthop. 34 (6) (2010) 869–875.
[152] H.B. Fan, J. Fu, X.D. Li, et al., Implantation of customized 3-D printed titanium prosthesis in limb salvage surgery: a case series and review of the literature, World J. Surg. Oncol. 13 (2015) 308.
[153] W. Wang, Z. Liang, S. Yang, et al., Three-dimensional (3D)-printed titanium sternum replacement: a case report, Thoracic Cancer 11 (11) (2020) 3375–3378.
[154] D.V.C. Stoffelen, K. Eraly, P. Debeer, The use of 3D printing technology in reconstruction of a severe glenoid defect: a case report with 2.5 years of follow-up, J. Shoulder Elbow Surg. 24 (8) (2015) E218–E222.
[155] L.L. Deng, X. Zhao, C. Wei, et al., Application of a three-dimensional printed segmental scapula prosthesis in the treatment of scapula tumors, J. Int. Med. Res. 47 (11) (2019) 5873–5882.
[156] Y. Zou, Y.Y. Yang, Q. Han, et al., Novel exploration of customized 3D printed shoulder prosthesis in revision of total shoulder arthroplasty A case report, Medicine (Baltim.) 97 (47) (2018), e13282.
[157] H. Liang, W. Guo, Y. Yang, et al., Efficacy and safety of a 3D-printed arthrodesis prosthesis for reconstruction after resection of the proximal humerus: preliminary outcomes with a minimum 2-year follow-up, BMC Muscoskel. Disord. 23 (2022) 635, https://doi.org/10.1186/s12891-022-05581-6.
[158] M.E.H. Boeckstyns, Wrist arthroplasty - a systematic review, Dan. Med. J. 61 (5) (2014).
[159] M.E.H. Boeckstyns, G. Herzberg, S. Merser, Favorable results after total wrist arthroplasty 65 wrists in 60 patients followed for 5-9 years, Acta Orthop. 84 (4) (2013) 415–419.
[160] J.A. Nydick, S.M. Greenberg, J.D. Stone, et al., Clinical outcomes of total wrist arthroplasty, J. Hand Surg. 37a (8) (2012) 1580–1584.
[161] O. Reigstad, T. Lutken, C. Grimsgaard, et al., Promising one- to six-year results with the Motec wrist arthroplasty in patients with post-traumatic osteoarthritis, Bone Joint Surg. Br. 94b (11) (2012) 1540–1545.
[162] O. Reigstad, T. Holm-Glad, R. Thorkildsen, et al., Successful conversion of wrist prosthesis to arthrodesis in 11 patients, J Hand Surg. Eur. 42 (1) (2017) 84–89.
[163] D. Palousek, J. Rosicky, D. Koutny, et al., Pilot study of the wrist orthosis design process, Rapid Prototyp. J. 20 (1) (2014) 27–32.
[164] M.X. Lu, L. Min, C. Xiao, et al., Uncemented three-dimensional-printed prosthetic replacement for giant cell tumor of distal radius: a new design of prosthesis and surgical techniques, Cancer Manag. Res. 10 (2018) 265–277.
[165] G. Chen, Y. Yin, C. Chen, Limb-salvage surgery using personalized 3D-printed porous tantalum prosthesis for distal radial osteosarcoma: a case report, Medicine (Baltim.) 100 (46) (2021).
[166] M.M. Xie, K.L. Tang, C.S. Yuan, 3D printing lunate prosthesis for stage IIIc Kienbock's disease: a case report, Arch. Orthop. Trauma Surg. 138 (4) (2018) 447–451.
[167] G.S. Xu, L. Gao, K. Tao, et al., Three-dimensional-printed upper limb prosthesis for a child with traumatic amputation of right wrist: a case report, Medicine (Baltim.) 96 (52) (2017) e9426.
[168] M. Lu, L. Min, C. Xiao, et al., Uncemented three-dimensional-printed prosthetic replacement for giant cell tumor of distal radius: a new design of prosthesis and surgical techniques, Cancer Manag. Res. 10 (2018) 265–277.
[169] Z.J. Ma, Z.F. Liu, Q.S. Shi, et al., Varisized 3D-printed lunate for kienbock's disease in different stages: preliminary results, Orthop. Surg. 12 (3) (2020) 792–801.
[170] C.G. Moran, R.T. Wenn, M. Sikand, et al., Early mortality after hip fracture: is delay before surgery important? J. Bone Joint Surg. Am. 87a (3) (2005) 483–489.
[171] C. Mauffrey, J.D. Hao, D.O. Cuellar, et al., The epidemiology and injury patterns of acetabular fractures: are the USA and China comparable? Clin. Orthop. 472 (11) (2014) 3332–3337.
[172] H. Zhang, Y. Liu, Q. Dong, et al., Novel 3D printed integral customized acetabular prosthesis for anatomical rotation center restoration in hip arthroplasty for developmental dysplasia of the hip crowe type III: a Case Report, Medicine (Baltim.) 99 (40) (2020), e22578.
[173] G.J. Hou, B.C. Liu, Y. Tian, et al., An innovative strategy to treat large metaphyseal segmental femoral bone defect using customized design and 3D printed micro-porous prosthesis: a prospective clinical study, J. Mater. Sci. Mater. Med. 31 (8) (2020).
[174] P. Upex, P. Jouffroy, G. Riouallon, Application of 3D printing for treating fractures of both columns of the acetabulum: benefit of pre-contouring plates on the mirrored healthy pelvis, Orthop. Traumatol. Surg. Res. 103 (3) (2017) 331–334.
[175] X.Z. Lin, X.L. Xiao, Y.M. Wang, et al., Biocompatibility of bespoke 3D-printed titanium alloy plates for treating acetabular fractures, BioMed Res. Int. (2018), 2053486.
[176] S.P. Narra, P.N. Mittwede, S.D. Wolf, et al., Additive manufacturing in total joint arthroplasty, Orthop. Clin. N. Am. 50 (1) (2019) 13–20.
[177] S.S. Wang, L. Wang, Y. Liu, et al., 3D printing technology used in severe hip deformity, Exp. Ther. Med. 14 (3) (2017) 2595–2599.
[178] M. Citak, L. Kochsiek, T. Gehrke, et al., Preliminary results of a 3D-printed acetabular component in the management of extensive defects, Hip Int. 28 (3) (2018) 266–271.
[179] M. Baauw, G.G. van Hellemondt, M. Spruit, A custom-made acetabular implant for paprosky type 3 defects, Orthopedics 40 (1) (2017) E195–E198.
[180] Y.B. Liu, H. Pan, L. Chen, et al., Total hip revision with custom-made spacer and prosthesis: a case report, World J Clin Cases 9 (25) (2021) 7605–7613.
[181] Y. Huang, Y.X. Zhou, H. Tian, et al., Minimum 7-year follow-up of A porous coated trabecular titanium cup manufactured with electron beam melting technique in primary total hip arthroplasty, Orthop. Surg. 13 (3) (2021) 817–824.
[182] E. Cavaignac, R. Pailhe, G. Laumond, et al., Evaluation of the accuracy of patient-specific cutting blocks for total knee arthroplasty: a meta-analysis, Int. Orthop. 39 (8) (2015) 1541–1552.
[183] S. Kurtz, K. Ong, E. Lau, et al., Projections of primary and revision hip and knee arthroplasty in the United States from 2005 to 2030, J. Bone Joint Surg. Am. 89a (4) (2007) 780–785.
[184] S.M. Kurtz, K.L. Ong, E. Lau, et al., International survey of primary and revision total knee replacement, Int. Orthop. 35 (12) (2011) 1783–1789.
[185] K. Thiele, C. Perka, G. Matziolis, et al., Current failure mechanisms after knee arthroplasty have changed: polyethylene wear is less common in revision surgery, J. Bone Joint Surg. Am. 97a (9) (2015) 715–720.
[186] W.C. Schroer, K.R. Berend, A.V. Lombardi, et al., Why are total knees failing today? Etiology of total knee revision in 2010 and 2011, J. Arthroplasty 28 (8) (2013) 116–119.
[187] A. Mannan, T.O. Smith, Favourable rotational alignment outcomes in PSI knee arthroplasty: a Level 1 systematic review and meta-analysis, Knee 23 (2) (2016) 186–190.

[188] J. Keenan, G. Chakrabarty, J.H. Newman, Treatment of supracondylar femoral fracture above total knee replacement by custom made hinged prosthesis, Knee 7 (3) (2000) 165–170.
[189] M. Ettinger, H. Windhagen, Individual revision arthroplasty of the knee joint, Orthopä 49 (5) (2020) 396–402.
[190] W.J. Liu, Z.W. Shao, S. Rai, et al., Three-dimensional-printed intercalary prosthesis for the reconstruction of large bone defect after joint-preserving tumor resection, J. Surg. Oncol. 121 (3) (2020) 570–577.
[191] A. Faizan, M. Bhowmik-Stoker, V. Alipit, et al., Development and verification of novel porous titanium metaphyseal cones for revision total knee arthroplasty, J. Arthroplasty 32 (6) (2017) 1946–1953.
[192] A.A. Cherny, A.N. Kovalenko, T.A. Kulyaba, et al., A prospective study on outcome of patient-specific cones in revision knee arthroplasty, Arch. Orthop. Trauma Surg. 141 (12) (2021) 2277–2286.
[193] Y. Ji, Y. Wu, J. Li, Use of three-dimensional–printed custom-made prosthesis to treat unicondylar femoral defect secondary to pathological fracture caused by giant cell tumor, J. Int. Med. Res. 49 (7) (2021), 03000605211025347.
[194] L.M. Ma, Y. Zhou, Y. Zhu, et al., 3D printed personalized titanium plates improve clinical outcome in microwave ablation of bone tumors around the knee, Sci. Rep. 7 (2017) 7626.
[195] M.X. Lu, J. Wang, F. Tang, et al., A three-dimensional printed porous implant combined with bone grafting following curettage of a subchondral giant cell tumour of the proximal tibia: a case report, BMC Surg. 19 (2019) 29.
[196] A.A. Cherny, A.N. Kovalenko, T.A. Kulyaba, et al., A prospective study on outcome of patient-specific cones in revision knee arthroplasty, Arch. Orthop. Trauma. Surg. 141 (12) (2021) 2277–2286.
[197] O. Gursan, M. Celtik, B. Yanik, et al., Three-Dimensionally-printed joint-preserving prosthetic reconstruction of massive bone defects after malignant tumor resection of the proximal tibia, Cureus 13 (3) (2021), e13784.
[198] Y. Zhang, M. Lu, L. Min, et al., Three-dimensional-printed porous implant combined with autograft reconstruction for giant cell tumor in proximal tibia, J. Orthop. Surg. Res. 16 (1) (2021) 2286.
[199] B. Hintermann, R. Ruiz, Total replacement of varus ankle three-component prosthesis design, Foot Ankle Clin. 24 (2) (2019) 305–324.
[200] P. Wardhani, P.I. Tsai, P.Y. Chen, et al., A computational study of different additive manufacturing-based total ankle replacement devices using three-dimensional human lower extremity models with various ankle postures, J. Mech. Med. Biol. 19 (2) (2019), 1940014.
[201] K.L. Apostle, T. Umran, M.J. Penner, Reimplantation of a totally extruded talus A case report, J Bone Joint Surg Am 92a (7) (2010) 1661–1665.
[202] M.M. Cohen, M. Kazak, Tibiocalcaneal arthrodesis with a porous tantalum spacer and locked intramedullary nail for post-traumatic global avascular necrosis of the talus, J. Foot Ankle Surg. 54 (6) (2015) 1172–1177.
[203] K.B. Lee, S.G. Cho, S.T. Jung, et al., Total ankle arthroplasty following revascularization of avascular necrosis of the talar body: two case reports and literature review, Foot Ankle Int. 29 (8) (2008) 852–858.
[204] H. Shnol, G.A. LaPorta, 3D printed total talar replacement A promising treatment option for advanced arthritis, avascular osteonecrosis, and osteomyelitis of the ankle, Clin. Podiatr. Med. Surg. 35 (4) (2018) 2403.
[205] X. Fang, H.Y. Liu, Y. Xiong, et al., Total talar replacement with a novel 3D printed modular prosthesis for tumors, Therapeut. Clin. Risk Manag. 14 (2018).
[206] M.E. Easley, S.B. Adams, W.C. Hembree, et al., Results of total ankle arthroplasty, J. Bone Joint Surg. Am. 93a (15) (2011) 1455–1468.
[207] Y. Yao, Z. Mo, G. Wu, et al., A personalized 3D-printed plate for tibiotalocalcaneal arthrodesis: design, fabrication, biomechanical evaluation and postoperative assessment, Comput. Biol. Med. 133 (2021), 104368.
[208] C. Belvedere, S. Siegler, A. Ensini, et al., Experimental evaluation of a new morphological approximation of the articular surfaces of the ankle joint, J. Biomech. 53 (2017) 97–104.
[209] C. Belvedere, S. Siegler, A. Fortunato, et al., New comprehensive procedure for custom-made total ankle replacements: medical imaging, joint modeling, prosthesis design, and 3D printing, J. Orthop. Res. 37 (3) (2019) 760–768.
[210] C.C. Akoh, J. Chen, S.B. Adams, Total ankle total talus replacement using a 3D printed talus component: a case report, J. Foot Ankle Surg. 59 (6) (2020) 1306–1312.
[211] C. Zhang, J. Cao, H. Zhu, et al., Endoscopic treatment of symptomatic foot and ankle bone cyst with 3D printing application, BioMed Res. Int. 2020 (2020), 8323658.
[212] D. Grau, A. Matamala, M. Bernaus, et al., A 3D-printed model of a titanium custom-made talus for the treatment of a chronic infection of the ankle, J. Foot Ankle Surg. 61 (1) (2022) 212–217.
[213] T.J. Dekker, J.R. Steele, A.E. Federer, et al., Use of patient-specific 3D-printed titanium implants for complex foot and ankle limb salvage, deformity correction, and arthrodesis procedures, Foot Ankle Int. 39 (8) (2018) 916–921.
[214] K.S. Hamid, S.G. Parekh, S.B. Adams, Salvage of severe foot and ankle trauma with a 3D printed scaffold, Foot Ankle Int. 37 (4) (2016) 433–439.
[215] M.D. Mu, Q.D. Yang, W. Chen, et al., Three dimension printing talar prostheses for total replacement in talar necrosis and collapse, Int. Orthop. 45 (9) (2021) 2313–2321.
[216] E. Provaggi, J.J.H. Leong, D.M. Kalaskar, Applications of 3D printing in the management of severe spinal conditions, Proc. Inst. Mech. Eng. H 231 (6) (2017) 471–486.
[217] F. Zhang, J. Liu, X. He, et al., Preclinical evaluation of a novel 3D-printed movable lumbar vertebral complex for replacement: in vivo and biomechanical evaluation of goat model, BioMed Res. Int. 2021 (2021), 2343404.
[218] V. Waran, V. Narayanan, R. Karuppiah, et al., Utility of multimaterial 3D printers in creating models with pathological entities to enhance the training experience of neurosurgeons Technical note, J. Neurosurg. 120 (2) (2014) 489–492.
[219] E.T.W. Tan, J.M. Ling, S.K. Dinesh, The feasibility of producing patient-specific acrylic cranioplasty implants with a low-cost 3D printer, J. Neurosurg. 124 (5) (2016) 1531–1537.
[220] W. van den Brink, N. Lamerigts, Complete osseointegration of a retrieved 3-D printed porous titanium cervical, Cage 7 (77) (2020) 526020.
[221] A. Senkoylu, I. Daldal, M. Cetinkaya, 3D printing and spine surgery, J. Orthop. Surg. 28 (2) (2020) 1–7.
[222] N.F. Xu, F. Wei, X.G. Liu, et al., Reconstruction of the upper cervical spine using a personalized 3D-printed vertebral body in an adolescent with ewing sarcoma, Spine 41 (1) (2016) E50–E54.
[223] J. Yang, H. Cai, J. Lv, et al., Biomechanical and histological evaluation of roughened surface titanium screws fabricated by electron beam melting, PLoS One 9 (4) (2014), e96179.
[224] Z.J. Zhang, H. Li, G.R. Fogel, et al., Finite element model predicts the biomechanical performance of transforaminal lumbar interbody fusion with various porous additive manufactured cages, Comput. Biol. Med. 95 (2018) 167–174.
[225] P.I. Tsai, C.C. Hsu, S.Y. Chen, et al., Biomechanical investigation into the structural design of porous additive manufactured cages using numerical and experimental approaches, Comput. Biol. Med. 76 (2016) 14–23.
[226] U. Spetzger, M. Frasca, S.A. Konig, Surgical planning, manufacturing and implantation of an individualized cervical fusion titanium cage using patient-specific data, Eur. Spine J. 25 (7) (2016) 2239–2246.
[227] A. Amelot, M. Colman, J.E. Loret, Vertebral body replacement using patient-specific three-dimensional-printed polymer implants in cervical spondylotic myelopathy: an encouraging preliminary report, Spine J. 18 (5) (2018) 892–899.
[228] M. Girolami, S. Boriani, S. Bandiera, et al., Biomimetic 3D-printed custom-made prosthesis for anterior column reconstruction in the thoracolumbar spine: a tailored option following en bloc resection for spinal tumors: preliminary results on a case-series of 13 patients, Eur. Spine J. 27 (12) (2018) 3073–3083.
[229] R.J. Mobbs, M. Coughlan, R. Thompson, et al., The utility of 3D printing for surgical planning and patient-specific implant design for complex spinal pathologies: case report, J. Neurosurg. Spine 26 (4) (2017) 513–518.
[230] W.J. Choy, R.J. Mobbs, B. Wilcox, et al., Reconstruction of the thoracic spine using a personalized 3D-printed vertebral body in an adolescent with a T9 primary bone tumour: case report, World Neurosurg 105 (2017).

[231] W.J. Choy, R.J. Mobbs, B. Wilcox, et al., Reconstruction of thoracic spine using a personalized 3D-printed vertebral body in adolescent with T9 primary bone tumor, World Neurosurg 105 (2017).
[232] X.C. Li, Y.G. Wang, Y.F. Zhao, et al., Multilevel 3D printing implant for reconstructing cervical spine with metastatic papillary thyroid carcinoma, Spine 42 (22) (2017) E1326–E1330.
[233] K.S. Chung, D.A. Shin, K.N. Kim, et al., Vertebral Reconstruction with Customized 3-Dimensional-Printed Spine Implant Replacing Large Vertebral Defect with 3-Year Follow-Up, 126, World Neurosurg, 2019, pp. 90–95.
[234] W. van den Brink, N. Lamerigts, Complete osseointegration of a retrieved 3-D printed porous titanium cervical cage, Front. Surg. 7 (2020), 526020.
[235] C. Dong, H. Wei, Y. Zhu, et al., Application of titanium alloy 3D-printed artificial vertebral body for stage III kummell's disease complicated by neurological deficits, Clin. Interv. Aging 15 (2020) 2265–2276.
[236] Y.Z. Jin, B. Zhao, X.D. Lu, et al., Mid- and long-term follow-up efficacy analysis of 3D-printed interbody fusion cages for anterior cervical discectomy and fusion, Orthop. Surg. 13 (7) (2021) 1969–1978.
[237] Q. Jian, Z. Liu, W. Duan, et al., Reconstruction of the cervical lateral mass using 3-dimensional-printed prostheses, Neurospine 19 (1) (2022) 202–211.
[238] C. Zoccali, J. Skoch, A. Patel, et al., The surgical neurovascular anatomy relating to partial and complete sacral and sacroiliac resections: a cadaveric, anatomic study, Eur. Spine J. 24 (5) (2015) 1109–1113.
[239] R. Madhu, R. Kotnis, A. Al-Mousawi, et al., Outcome of surgery for reconstruction of fractures of the acetabulum - the time dependent effect of delay, Bone Joint Surg. Br 88b (9) (2006) 1197–1203.
[240] S.E. Puchner, P.T. Funovics, C. Bohler, et al., Oncological and surgical outcome after treatment of pelvic sarcomas, PLoS One 12 (2) (2017), e0172203.
[241] O.L.A. Harrysson, D.J. Marcellin-Little, T.J. Horn, Applications of metal additive manufacturing in veterinary orthopedic surgery, Jom 67 (3) (2015) 647–654.
[242] J. Tao, Design,Production and clinical application of custom total hip prosthesis, J. Biomed. Eng. 22 (2) (2005) 2392.
[243] X.J. Chen, L. Xu, Y.P. Wang, et al., Image-guided installation of 3D-printed patient-specific implant and its application in pelvic tumor resection and reconstruction surgery, Comput. Methods Progr. Biomed. 125 (2016) 66–78.
[244] J.W. Park, H.G. Kang, J.H. Kim, et al., The application of 3D-printing technology in pelvic bone tumor surgery, J. Orthop. Sci. 26 (2) (2021) 276–283.
[245] W. Peng, R. Zheng, H. Wang, et al., Reconstruction of bony defects after tumor resection with 3D-printed anatomically conforming pelvic prostheses through a novel treatment strategy, BioMed Res. Int. 2020 (2020), 8513070.
[246] G.L. Rosa, C. Clienti, S.D. Bella, et al., Numerical analysis of a custom-made pelvic prosthesis, Procedia Struct. Integr. 2 (2016) 1295–1302.
[247] L. Xu, H. Qin, J. Tan, et al., Clinical study of 3D printed personalized prosthesis in the treatment of bone defect after pelvic tumor resection, J Orthop Translat 29 (2021) 163–169.
[248] D. Wang, Y.M. Wang, S.B. Wu, et al., Customized a Ti6Al4V bone plate for complex pelvic fracture by selective laser melting, Materials 10 (1) (2017) 2035.
[249] X. Zhao, J.L. Xiao, Y. Sun, et al., Novel 3D printed modular hemipelvic prosthesis for successful hemipelvic arthroplasty: a case study, J. Bionic. Eng. 15 (6) (2018) 1067–1074.
[250] H. Liang, T. Ji, Y. Zhang, et al., Reconstruction with 3D-printed pelvic endoprostheses after resection of a pelvic tumour, Bone Joint Lett. J 99b (2) (2017) 267–275.
[251] T. Ji, W. Guo, R.L. Yang, et al., Modular hemipelvic endoprosthesis reconstruction-Experience in 100 patients with mid-term follow-up results, Ejso 39 (1) (2013) 53–60.
[252] D. Kim, J.Y. Lim, K.W. Shim, et al., Sacral reconstruction with a 3D-printed implant after hemisacrectomy in a patient with sacral osteosarcoma: 1-year follow-up result, Yonsei Med. J. 58 (2) (2017) 453–457.
[253] J.W. Park, H.G. Kang, J.H. Kim, et al., The application of 3D-printing technology in pelvic bone tumor surgery, J. Orthop. Sci. 26 (2) (2021) 276–283.
[254] M. Javaid, A. Haleem, Current status and challenges of Additive manufacturing in orthopaedics: an overview, Journal of Clinical Orthopaedics and Trauma 10 (2) (2019) 380–386.
[255] S.W. Mok, R. Nizak, S.C. Fu, et al., From the printer: potential of three-dimensional printing for orthopaedic applications, Journal of Orthopaedic Translation 6 (2016) 42–49.
[256] K.C. Nune, R.D.K. Misra, S.J. Li, et al., Cellular response of osteoblasts to low modulus Ti-24Nb-4Zr-8Sn alloy mesh structure, J. Biomed. Mater. Res. 105 (3) (2017) 859–870.
[257] N. Hafeez, J. Liu, L. Wang, et al., Superelastic response of low-modulus porous beta-type Ti-35Nb-2Ta-3Zr alloy fabricated by laser powder bed fusion, Addit. Manuf. 34 (2020), 101264.
[258] A.N. Alagha, S. Hussain, W. Zaki, Additive manufacturing of shape memory alloys: a review with emphasis on powder bed systems, Mater. Des. 204 (2021), 109654.
[259] M.S. Safavi, A. Bordbar-Khiabani, J. Khalil-Allafi, et al., Additive manufacturing: an opportunity for the fabrication of near-net-shape NiTi implants, Journal of Manufacturing and Materials Processing 6 (3) (2022) 2065.
[260] C. Haberland, M. Elahinia, J.M. Walker, et al., On the development of high quality NiTi shape memory and pseudoelastic parts by additive manufacturing, Smart Mater. Struct. 23 (2014).
[261] M. Elahinia, N. Shayesteh Moghaddam, M. Taheri Andani, et al., Fabrication of NiTi through additive manufacturing: a review, Prog. Mater. Sci. 83 (2016) 630–663.
[262] B. Lu, X. Cui, W. Ma, et al., Promoting the heterogeneous nucleation and the functional properties of directed energy deposited NiTi alloy by addition of La2O3, Addit. Manuf. 33 (2020) 101150.
[263] A. Bandyopadhyay, B.V. Krishna, W. Xue, et al., Application of laser engineered net shaping (LENS) to manufacture porous and functionally graded structures for load bearing implants, J. Mater. Sci. Mater. Med. 20 (Suppl 1) (2009) S29–S34.
[264] M. Taheri Andani, C. Haberland, J.M. Walker, et al., Achieving biocompatible stiffness in NiTi through additive manufacturing, J. Intell. Mater. Syst. Struct. 27 (19) (2016) 2661–2671.
[265] D.K. Mishra, P.M. Pandey, Mechanical behaviour of 3D printed ordered pore topological iron scaffold, Mater. Sci. Eng. 783 (2020), 139293.
[266] P. Sharma, P.M. Pandey, Corrosion behaviour of the porous iron scaffold in simulated body fluid for biodegradable implant application, Mat. Sci. Eng. C-Mater. 99 (2019) 838–852.
[267] N.E. Putra, M.J. Mirzaali, I. Apachitei, et al., Multi-material additive manufacturing technologies for Ti-, Mg-, and Fe-based biomaterials for bone substitution, Acta Biomater. 109 (2020).
[268] D.K. Mishra, P.M. Pandey, Effects of morphological characteristics on the mechanical behavior of 3D printed ordered pore topological Fe scaffold, Mater. Sci. Eng. 804 (2021), 140759.
[269] R. Karunakaran, S. Ortgies, A. Tamayol, et al., Additive manufacturing of magnesium alloys, Bioact. Mater. 5 (1) (2020) 44–54.
[270] X.T. Zhang, J. Mao, Y.F. Zhou, et al., Mechanical properties and osteoblast proliferation of complex porous dental implants filled with magnesium alloy based on 3D printing, J. Biomater. Appl. 35 (10) (2020) 1275–1283.
[271] J. Dong, Y. Li, P. Lin, et al., Solvent-cast 3D printing of magnesium scaffolds, Acta Biomater. 114 (2020) 497–514.
[272] K. Xie, N. Wang, Y. Guo, et al., Additively manufactured biodegradable porous magnesium implants for elimination of implant-related infections: an in vitro and in vivo study, Bioact. Mater. 8 (2022) 140–152.
[273] Y. Li, W. Li, F.S.L. Bobbert, et al., Corrosion fatigue behavior of additively manufactured biodegradable porous zinc, Acta Biomater. 106 (2020) 439–449.
[274] H. Kabir, K. Munir, C. Wen, et al., Recent research and progress of biodegradable zinc alloys and composites for biomedical applications: biomechanical and biocorrosion perspectives, Bioact. Mater. 6 (3) (2021) 836–879.
[275] D. Zhao, C. Han, B. Peng, et al., Corrosion fatigue behavior and anti-fatigue mechanisms of an additively manufactured biodegradable zinc-magnesium gyroid scaffold, Acta Biomater. (2022).
[276] I. Cockerill, Y. Su, S. Sinha, et al., Porous zinc scaffolds for bone tissue engineering applications: a novel additive manufacturing and casting approach, Mater. Sci. Eng. C 110 (2020), 110738.

[277] D. Xia, Y. Qin, H. Guo, et al., Additively manufactured pure zinc porous scaffolds for critical-sized bone defects of rabbit femur, Bioact. Mater. 19 (2023) 12–23.
[278] K. Lietaert, A.A. Zadpoor, M. Sonnaert, et al., Mechanical properties and cytocompatibility of dense and porous Zn produced by laser powder bed fusion for biodegradable implant applications, Acta Biomater. 110 (2020) 289–302.
[279] D.T. Chou, D. Wells, D. Hong, et al., Novel processing of iron-manganese alloy-based biomaterials by inkjet 3-D printing, Acta Biomater. 9 (10) (2013) 8593–8603.
[280] D.H. Hong, D.T. Chou, O.I. Velikokhatnyi, et al., Binder-jetting 3D printing and alloy development of new biodegradable Fe-Mn-Ca/Mg alloys, Acta Biomater. 45 (2016) 375–386.
[281] C. Yang, Z.G. Huan, X.Y. Wang, et al., 3D printed Fe scaffolds with HA nanocoating for bone regeneration, ACS Biomater. Sci. Eng. 4 (2) (2018) 608–616.
[282] P. Sharma, P.M. Pandey, Morphological and mechanical characterization of topologically ordered open cell porous iron foam fabricated using 3D printing and pressureless microwave sintering, Mater. Des. 160 (2018) 442–454.
[283] J.V. Bondareva, O.N. Dubinin, Y.O. Kuzminova, et al., Biodegradable iron-silicon implants produced by additive manufacturing, Biomed Mater 17 (3) (2022).
[284] C.C. Ng, M.M. Savalani, H.C. Man, et al., Layer manufacturing of magnesium and its alloy structures for future applications, Virtual Phys. Prototyp. 5 (1) (2010) 13–19.
[285] V.S. Telang, R. Pemmada, V. Thomas, et al., Harnessing additive manufacturing for magnesium-based metallic bioimplants: recent advances and future perspectives, Current Opinion in Biomedical Engineering 17 (2021), 100264.
[286] M. Salehi, S. Maleksaeedi, S.M.L. Nai, et al., A paradigm shift towards compositionally zero-sum binderless 3D printing of magnesium alloys via capillary-mediated bridging, Acta Mater. 165 (2019) 294–306.
[287] M. Salehi, S. Maleksaeedi, M.A. Bin Sapari, et al., Additive manufacturing of magnesium-zinc-zirconium (ZK) alloys via capillary-mediated binderless three-dimensional printing, Mater. Des. 169 (2019), 107683.
[288] X. Zhang, J. Mao, Y. Zhou, et al., Mechanical properties and osteoblast proliferation of complex porous dental implants filled with magnesium alloy based on 3D printing, J. Biomater. Appl. 35 (10) (2021) 1275–1283.
[289] Y. Zhang, T. Lin, H. Meng, et al., 3D gel-printed porous magnesium scaffold coated with dibasic calcium phosphate dihydrate for bone repair in vivo, J Orthop Translat 33 (2022) 13–23.
[290] C.R. Alcala-Orozco, I. Mutreja, X. Cui, et al., Hybrid biofabrication of 3D osteoconductive constructs comprising Mg-based nanocomposites and cell-laden bioinks for bone repair, Bone 154 (2021), 116198.
[291] C. Liu, C. Ling, C. Chen, et al., Laser additive manufacturing of magnesium alloys and its biomedical applications, MS 1 (4) (2022).
[292] I. Cockerill, Y. Su, S. Sinha, et al., Porous zinc scaffolds for bone tissue engineering applications: a novel additive manufacturing and casting approach, Mater Sci Eng C Mater Biol Appl 110 (2020), 110738.
[293] Y. Zhou, J. Wang, Y. Yang, et al., Laser additive manufacturing of zinc targeting for biomedical application, Int J Bioprint 8 (1) (2022) 2501.
[294] K.H. Leitz, C. Grohs, P. Singer, et al., Fundamental analysis of the influence of powder characteristics in Selective Laser Melting of molybdenum based on a multi-physical simulation model, Int. J. Refract. Metals Hard Mater. 72 (2018) 1–8.
[295] K. Halada, K. Minagawa, K. Chiba, et al., Solidified Microstructure of Zn-Al Alloy Powders Produced by Various Atomization Methods, 40, 1993, pp. 1160–1165.
[296] Q. Yang, Y.T. Liu, J. Liu, et al., Microstructure evolution of the rapidly solidified alloy powders and composite powders, Mater. Des. 182 (2019), 108045.
[297] P. Sungkhaphaitoon, T. Plookphol, S. Wisutmethangoon, et al., Design and Development of a Centrifugal Atomizer for Producing Zinc Metal Powder, 2012, pp. 77–82.
[298] P. Wen, M. Voshage, L. Jauer, et al., Laser additive manufacturing of Zn metal parts for biodegradable applications: processing, formation quality and mechanical properties, Mater, Design 155 (2018) 36–45.
[299] Y. Chen, P. Wen, M. Voshage, et al., Laser additive manufacturing of Zn metal parts for biodegradable implants: effect of gas flow on evaporation and formation quality, J. Laser Appl. 31 (2) (2019), 022304.
[300] Y. Yang, M. Yang, C. He, et al., Rare Earth Improves Strength and Creep Resistance of Additively Manufactured Zn Implants, Composites Part B: Engineering 216, 2021, 108882.
[301] M. Yang, Y. Shuai, Y. Yang, et al., In situ grown rare earth lanthanum on carbon nanofibre for interfacial reinforcement in Zn implants, Virtual Phys. Prototyp. 17 (3) (2022) 700–717.
[302] S. Leng, K. McGee, J. Morris, et al., Anatomic modeling using 3D printing: quality assurance and optimization, 3D Print, Med 3 (1) (2017) 6.
[303] B.E. Carroll, T.A. Palmer, A.M. Beese, Anisotropic tensile behavior of Ti-6Al-4V components fabricated with directed energy deposition additive manufacturing, Acta Mater. 87 (2015) 309–320.
[304] S. Waheed, J.M. Cabot, N.P. Macdonald, et al., 3D printed microfluidic devices: enablers and barriers, Lab Chip 16 (11) (2016) 1993–2013.
[305] J.T. Lambrecht, D.C. Berndt, R. Schumacher, et al., Generation of three-dimensional prototype models based on cone beam computed tomography, Int. J. Comput. Assist. Radiol. Surg. 4 (2) (2009) 175–180.
[306] A. Marro, T. Bandukwala, W. Mak, Three-dimensional printing and medical imaging: a review of the methods and applications, Curr. Probl. Diagn. Radiol. 45 (1) (2016) 2.
[307] Q. Lan, A. Chen, T. Zhang, et al., Development of three-dimensional printed craniocerebral models for simulated neurosurgery, World Neurosurg 91 (2016) 434–442.
[308] J.P. Thawani, J.M. Pisapia, N. Singh, et al., Three-Dimensional Printed Modeling of an Arteriovenous Malformation Including Blood Flow, 90, World Neurosurg, 2016, pp. 675–683.
[309] R. Xu, Z.H. Wang, T.J. Ma, et al., Effect of 3D printing individualized ankle-foot orthosis on plantar biomechanics and pain in patients with plantar fasciitis: a randomized controlled trial, Med. Sci. Mon. Int. Med. J. Exp. Clin. Res. 25 (2019) 1392–1400.
[310] X. Geng, Y. Li, F. Li, et al., A new 3D printing porous trabecular titanium metal acetabular cup for primary total hip arthroplasty: a minimum 2-year follow-up of 92 consecutive patients (vol 15, 383, 2020), J. Orthop. Surg. 15 (1) (2020) 2383.
[311] C.B. Wang, Y.H. Chen, L.P. Wang, et al., Three-dimensional printing of patient-specific plates for the treatment of acetabular fractures involving quadrilateral plate disruption, BMC Muscoskel. Disord. 21 (1) (2020) 2451.
[312] J. Witowski, M. Sitkowski, T. Zuzak, et al., From ideas to long-term studies: 3D printing clinical trials review, Int. J. Comput. Assist. Radiol. Surg. 13 (9) (2018) 1473–1478.
[313] L.M. Ricles, J.C. Coburn, M. Di Prima, et al., Regulating 3D-printed medical products, Sci. Transl. Med. 10 (461) (2018) 6521.
[314] R.J. Morrison, K.N. Kashlan, C.L. Flanangan, et al., Regulatory considerations in the design and manufacturing of implantable 3D-printed medical devices, Clin. Transl. Sci. 8 (5) (2015) 594–600.
[315] C. Shorten, T.M. Khoshgoftaar, A survey on image data augmentation for deep learning, Journal of Big Data 6 (1) (2019) 2060.
[316] M.A. Mahmood, A.I. Visan, C. Ristoscu, et al., Artificial Neural Network Algorithms for 3D Printing 14 (1) (2021) 2163.
[317] M. Shirmohammadi, S.J. Goushchi, P.M. Keshtiban, Optimization of 3D printing process parameters to minimize surface roughness with hybrid artificial neural network model and particle swarm algorithm, Progress in Additive Manufacturing 6 (2) (2021) 199–215.
[318] L. Yan, J.L. Lim, J.W. Lee, et al., Finite element analysis of bone and implant stresses for customized 3D-printed orthopaedic implants in fracture fixation, Med. Biol. Eng. Comput. 58 (5) (2020) 921–931.
[319] D.J. Roach, A. Rohskopf, C.M. Hamel, et al., Utilizing computer vision and artificial intelligence algorithms to predict and design the mechanical compression response of direct ink write 3D printed foam replacement structures, Addit. Manuf. 41 (2021), 101950.
[320] C. Haberland, M. Elahinia, J.M. Walker, et al., On the development of high quality NiTi shape memory and pseudoelastic parts by additive manufacturing, Smart Mater. Struct. 23 (10) (2014), 104002.
[321] J.M. Walker, C. Haberland, M.T. Andani, et al., Process development and characterization of additively manufactured nickel-titanium shape memory parts, J. Intell. Mater. Syst. Struct. 27 (19) (2016) 2653–2660.

[322] T. Habijan, C. Haberland, H. Meier, et al., The biocompatibility of dense and porous Nickel-Titanium produced by selective laser melting, Mat. Sci. Eng. C-Mater. 33 (1) (2013) 419–426.
[323] C. Micolini, F.B. Holness, J.A. Johnson, et al., Assessment of embedded conjugated polymer sensor arrays for potential load transmission measurement in orthopaedic implants, Sensors 17 (12) (2017) 2786.
[324] J.K. Chang, H.P. Chang, Q. Guo, et al., Biodegradable electronic systems in 3D, heterogeneously integrated formats, Adv. Mater. 30 (11) (2018), 1704955.
[325] A. Basir, H. Yoo, A stable impedance-matched ultrawideband antenna system mitigating detuning effects for multiple biotelemetric applications, IEEE Trans. Antenn. Propag. 67 (5) (2019) 3416–3421.
[326] C.S. Park, T.H. Ha, M. Kim, et al., Fast and sensitive near-infrared fluorescent probes for ALP detection and 3d printed calcium phosphate scaffold imaging in vivo, Biosens. Bioelectron. 105 (2018) 151–158.
[327] J. Qin, D.Q. Yang, S. Maher, et al., Micro- and nano-structured 3D printed titanium implants with a hydroxyapatite coating for improved osseointegration, J. Mater. Chem. B 6 (19) (2018) 3136–3144.
[328] J.Y. Park, J.H. Shim, S.A. Choi, et al., 3D printing technology to control BMP-2 and VEGF delivery spatially and temporally to promote large-volume bone regeneration, J. Mater. Chem. B 3 (27) (2015) 5415–5425.
[329] W.H. Zhang, W. Shi, S.H. Wu, et al., 3D printed composite scaffolds with dual small molecule delivery for mandibular bone regeneration, Biofabrication 12 (3) (2020), 035020.
[330] F.Y. Teng, I.C. Tai, M.L. Ho, et al., Controlled release of BMP-2 from titanium with electrodeposition modification enhancing critical size bone formation, Mat. Sci. Eng. C-Mater. 105 (2019), 109879.
[331] B.N. Teixeira, P. Aprile, R.H. Mendonca, et al., Evaluation of bone marrow stem cell response to PLA scaffolds manufactured by 3D printing and coated with polydopamine and type I collagen, J. Biomed. Mater. Res. B 107 (1) (2019) 37–49.
[332] L. Chen, L.P. Shao, F.P. Wang, et al., Enhancement in sustained release of antimicrobial peptide and BMP-2 from degradable three dimensional-printed PLGA scaffold for bone regeneration, Rsc Adv 9 (19) (2019) 10494–10507.
[333] L.M. Ma, S. Cheng, X.F. Ji, et al., Immobilizing magnesium ions on 3D printed porous tantalum scaffolds with polydopamine for improved vascularization and osteogenesis, Mat. Sci. Eng. C-Mater. 117 (2020) 111303.
[334] T. Zhang, W.H. Zhou, Z.J. Jia, et al., Polydopamine-assisted functionalization of heparin and vancomycin onto microarc-oxidized 3D printed porous Ti6Al4V for improved hemocompatibility, osteogenic and anti-infection potencies, Science China-Materials 61 (4) (2018) 579–592.
[335] L.J. Yu, Y.H. Wu, J.Y. Liu, et al., 3D culture of bone marrow-derived mesenchymal stem cells (BMSCs) could improve bone regeneration in 3D-printed porous Ti6Al4V scaffolds, Stem Cell. Int. (2018), 2074021.
[336] W. Zhang, C.G. Sun, J.X. Zhu, et al., 3D printed porous titanium cages filled with simvastatin hydrogel promotes bone ingrowth and spinal fusion in rhesus macaques, Biomater. Sci. 8 (15) (2020) 4147–4156.
[337] W.G. Wu, C.Y. Ye, Q.X. Zheng, et al., A therapeutic delivery system for chronic osteomyelitis via a multi-drug implant based on three-dimensional printing technology, J. Biomater. Appl. 31 (2) (2016) 250–260.
[338] Y.L. Zhang, D. Zhai, M.C. Xu, et al., 3D-printed bioceramic scaffolds with a Fe3O4/graphene oxide nanocomposite interface for hyperthermia therapy of bone tumor cells, J. Mater. Chem. B 4 (17) (2016) 2874–2886.
[339] J.Y. Li, L.L. Li, J. Zhou, et al., 3D printed dual-functional biomaterial with self-assembly micro-nano surface and enriched nano argentum for antibalctorial and bone regeneration, Appl. Mater. Today 17 (2019) 206–215.